Limited variation between SARS-CoV-2-infected individuals in domain specificity and relative potency of the antibody response against the spike glycoprotein

Hanora A. Van Ert[1], Dana W. Bohan[1], Kai Rogers[1], Mohammad Fili[2], Roberth A. Rojas Chávez[1], Enya Qing[3], Changze Han[1], Spencer Dempewolf[1], Guiping Hu[2], Nathan Schwery[1], Kristina Sevcik[1], Natalie Ruggio[1], Devlin Boyt[1], Michael A. Pentella[4], Tom Gallagher[3], J. Brooks Jackson[5], Anna E. Merrill[5], C. Michael Knudson[5], Grant D. Brown[6], Wendy Maury[1], and Hillel Haim[1#]

[1] Department of Microbiology and Immunology, The University of Iowa, Iowa City, IA
[2] Department of Industrial and Manufacturing Systems Engineering, Iowa State University, Ames, IA
[3] Department of Microbiology and Immunology, Loyola University Chicago, Maywood, IL
[4] State Hygienic Laboratory, The University of Iowa, Iowa City, IA
[5] Department of Pathology, University of Iowa Hospitals & Clinics, Iowa City, IA
[6] Department of Biostatistics, School of Public Health, The University of Iowa, Iowa City, IA

[#] To whom correspondence should be addressed:
Hillel Haim, MD, PhD
Department of Microbiology and Immunology
The University of Iowa
51 Newton Rd, 3-770 BSB
Iowa City, Iowa, 52242
Phone: (319) 335-9989
Email: Hillel-haim@uiowa.edu

Short Title: Variation in antibody responses against SARS-CoV-2

Keywords: SARS-CoV-2, COVID-19, spike protein, convalescent plasma, antibody neutralization, immunoassay, immunoglobulins.

Abstract word count: 250.

Text word count: 6,975.

ABSTRACT

The spike protein of SARS-CoV-2 is arranged as a trimer on the virus surface, composed of three S1 and three S2 subunits. Infected and vaccinated individuals generate antibodies against spike, which can neutralize the virus. Most antibodies target the receptor-binding domain (RBD) and N-terminal domain (NTD) of S1; however, antibodies against other regions of spike have also been isolated. The variation between infected individuals in domain specificity of the antibodies and in their relative neutralization efficacy is still poorly characterized. To this end, we tested serum and plasma samples from 85 COVID-19 convalescent subjects using 7 immunoassays that employ different domains, subunits and oligomeric forms of spike to capture the antibodies. Samples were also tested for their neutralization of pseudovirus containing SARS-CoV-2 spike and of replication-competent SARS-CoV-2. We observed strong correlations between the levels of NTD- and RBD-specific antibodies, with a fixed ratio of each type to all anti-spike antibodies. The relative potency of the response (defined as the measured neutralization efficacy relative to the total level of spike-targeting antibodies) also exhibited limited variation between subjects, and was not associated with the overall amount of anti-spike antibodies produced. Accordingly, the ability of immunoassays that use RBD, NTD and different forms of S1 or S1/S2 as capture antigens to estimate the neutralizing efficacy of convalescent samples was largely similar. These studies suggest that host-to-host variation in the polyclonal response elicited against SARS-CoV-2 spike is primarily limited to the quantity of antibodies generated rather than their domain specificity or relative neutralization potency.

IMPORTANCE

Infection by SARS-CoV-2 elicits antibodies against various domains of the spike protein, including the RBD, NTD and S2. Different infected individuals generate vastly different amounts of anti-spike antibodies. By contrast, as we show here, there is a remarkable similarity in the properties of the antibodies produced. Different individuals generate the same proportions of antibodies against each domain of the spike protein. Furthermore, the relationship between the amount of anti-spike antibodies produced and their neutralization efficacy of SARS-CoV-2 is highly conserved. Therefore, the observed variation in the neutralizing activity of the antibody response in COVID-19 convalescent subjects is caused by differences in the amounts of antibodies rather than their recognition properties or relative antiviral activity. These findings suggest that COVID-19 vaccine strategies that focus on enhancing the overall level of the antibodies will likely elicit a more uniformly efficacious protective response.

INTRODUCTION

The spike protein on the surface of SARS-CoV-2 mediates fusion with target cells (1, 2). Spike is generated as a precursor that is cleaved by furin in the producer cells to generate S1 and S2 subunits (3). These subunits are non-covalently associated on the virus surface, where they form a trimer of heterodimers (4). Furin cleavage primes spike for further processing by the serine protease TMPRSS2 on the plasma membrane or the cysteine protease cathepsin L within the endosome (3, 5, 6). Spike is highly immunogenic in humans and, in infected and vaccinated individuals, readily elicits antibodies that play a critical role in protection (7, 8). Most neutralizing antibodies isolated to date target the receptor-binding domain (RBD) on the S1 subunit (9-15). In addition, multiple neutralizing antibodies that target the N-terminal domain (NTD) of S1 have been isolated (16-18). By contrast, neutralizing antibodies against the C-terminal domain (CTD) of S1 or against the S2 subunit are relatively rare (19, 20). The variation between individuals in the domain specificity of the anti-spike response and in the relative neutralization efficacy of the antibodies produced remains poorly explored.

To address this question, we quantified the binding specificity of anti-spike antibodies in 85 convalescent COVID-19 serum and plasma samples using capture antigens that represent different domains, subunits, and oligomeric forms of spike. A panel of 7 in-house and commercial immunoassays that quantify anti-spike antibodies was tested, as well as a nucleocapsid-based assay. Antibody content in the samples measured by these assays was compared with their neutralization efficacy of SARS-CoV-2. We observed that different subjects exhibit remarkably similar ratios of anti-RBD and anti-NTD antibodies relative to the total anti-spike antibodies. Interestingly, the relative potency of the convalescent samples (defined as the ratio between neutralization efficacy and the amount of anti-spike antibodies measured) was also similar in different individuals, and was not associated with the robustness of the response against spike. Our results demonstrate limited host-to-host variation in both spike domain

specificity and in the relative potency of the antibody response elicited after SARS-CoV-2 infection. Variation between hosts in the polyclonal response generated is primarily limited to the quantity of the antibodies rather than the domains targeted or the efficacy of their neutralizing activity.

RESULTS

Strong correlations between results of immunoassays that apply different spike components as the capture antigen

To determine the target specificity of the SARS-CoV-2 antibody response, we analyzed serum and plasma samples collected from individuals who had recovered from COVID-19 (see all donor information in **Supp. Table S1**). Serum samples were obtained from individuals willing to donate convalescent plasma for the treatment of COVID-19 patients. In addition, we analyzed plasma samples from obstetric patients who had serologic evidence of COVID-19 infection; samples were collected during their hospitalization for delivery (21). All samples were collected between March 2020 and January 2021. None of the donors required hospitalization for COVID-19-related symptoms. For 68% of donors, the precise date of positivity for SARS-CoV-2 (by PCR analysis of a nasopharyngeal swab) was known; among these subjects, 82% of the serum or plasma samples were collected within 60 days of the positive PCR result (**Supp. Fig. S1A**). For each serum or plasma sample, we quantified the levels of SARS-CoV-2-specific antibodies using commercially-available and in-house-developed immunoassays that apply different domains, subunits or oligomeric forms of the spike protein as the capture antigen (**Table 1** and **Fig. 1A**). To mimic the native spike trimer on the virus surface, we used a cell-based enzyme linked immunosorbent assay (cbELISA) that measures antibodies against the full-length membrane-bound form of spike (22-24). For this purpose, we used human osteosarcoma (HOS)

cells that express on their surface fusion-competent spike trimers by transfection with an expression plasmid that encodes the full-length protein. Samples were also tested by ELISAs, in which recombinant soluble dimeric forms of the RBD, NTD or the complete ectodomain of S1/S2 (designated Ecto) were used as the capture antigens. The Ecto protein was generated by abrogating the furin cleavage site at spike positions 682-685 (3). Binding of antibodies in serum or plasma to these antigens was measured using a secondary antibody specific for the human kappa light chain, which detects isotypes IgG, IgM and IgA. In addition, we tested the samples with commercial immunoassays that detect IgG against the S1 subunit (Ortho Vitros), S1/S2 subunits (DiaSorin Liaison IgG) and a trimeric soluble form of S1/S2 (DiaSorin TrimericS IgG). To quantify non-spike-targeting antibodies elicited against SARS-CoV-2, we used the Roche assay that measures total antibodies against the nucleocapsid protein of SARS-CoV-2. Given that our study focused on quantitative relationships between antibody levels and neutralization efficacies, we excluded from the analyses all samples that were negative for SARS-CoV-2 antibodies in at least 5 of the 8 immunoassays. Our final test set was composed of 85 samples (57 serum and 28 plasma). The Ortho test was only performed with the 57 serum samples due to assay incompatibility with plasma.

The RBD, NTD and Ecto ELISAs, as well as cbELISA showed a normal distribution of their $\log_{10}$-transformed values (see **Fig. 1B** and results of a Shapiro-Wilk test in **Supp. Fig. S1B**). The $\log_{10}$-transformed values of the Liaison and TrimericS tests were also normally distributed, whereas the Roche test showed no evidence for normality (**Supp. Fig. S1B** and **S1C**). We compared values measured in the different assays using the non-parametric Spearman rank test. Strong correlations were observed between values measured in the assays that apply different spike components as the capture antigens, whereas correlations with the nucleocapsid-based Roche assay were less strong (**Fig. 1C** and **Supp. Fig. S2**).

Interestingly, a strong association was observed between the content of antibodies against the non-overlapping NTD and RBD of spike (**Fig. 1D**).

Previous studies have suggested that the majority of spike-targeting antibodies elicited after infection or vaccination target the RBD and NTD, whereas antibodies that target the CTD and S2 are less common (25, 26). We used our in-house ELISA assays to determine the relative amounts of antibodies against the RBD and NTD of spike. Since equimolar concentrations of the NTD, RBD and Ecto proteins were used for capture in our ELISAs, we first compared for each sample the sum of the ELISA values measured in the RBD and NTD assays with the value measured for Ecto. We observed that for each sample, the sum of the NTD and RBD values was comparable to that of Ecto, indicating that antibodies against the NTD and RBD account for the vast majority of all S1/S2-targeting antibodies (**Fig. 1E**). We further compared the level of antibodies that target the RBD and NTD by calculating for each patient the ratio between the values in these assays. Greater binding activity to the RBD than NTD was observed, with a mean RBD-to-NTD ratio of 1.8 and standard deviation of 0.99 (**Fig. 1F**). Thus, the ratio of RBD-to-NTD antibodies was relatively constant in different subjects, ranging between 1 and 3 in 78% of cases. Only 2% of the samples showed two-fold or higher binding to the NTD, and only 8% of the samples showed more than 3-fold higher binding to the RBD. The proportion of RBD- or NTD-targeting antibodies (relative to all spike-targeting antibodies) did not vary with the interval between infection and the time of sample collection (**Supp. Fig. S3**).

Therefore, the levels of antibodies elicited against the RBD and NTD are highly correlated. Antibodies targeting the two domains exhibit a relatively constant relationship and account for the vast majority of all anti-spike antibodies elicited.

Different domains, subunits and oligomeric forms of spike show similar abilities to estimate the neutralization efficacy of COVID-19 convalescent samples

Neutralizing antibodies mainly target the RBD and NTD of spike (9, 16, 17). Previous studies have shown that the levels of antibodies against different forms of spike (including S1, S1/S2 and RBD) correlate well with the neutralization capacity of the samples (27-31). However, the relationship between the neutralization activity of the polyclonal response in each individual and its domain specificity, as well as the variation in this relationship between different hosts are still poorly characterized. To address these questions, we compared the neutralization efficacy of the convalescent samples and their binding to the capture antigens that represent different domains and forms of spike. To quantify neutralization, we first used a replication-defective pseudovirus that contains the spike protein of SARS-CoV-2. For this purpose, we generated vesicular stomatitis virus (VSV) pseudovirions that encode the firefly luciferase gene in place of the native VSV-G glycoprotein gene and are pseudotyped with SARS-CoV-2 spike (VSV-SARS2-S) (5, 32). Residual infectivity of the pseudovirus in the presence of sera was measured using Vero-E6 target cells. The calculated dilution of sera at which virus infectivity was reduced two-fold is reported as the IC_{50} value. The $\log_{10}$-transformed IC_{50} values were consistent with a normal distribution (*P* value = 0.329 in a Shapiro-Wilk test), with a median IC_{50} corresponding to a dilution of 1:914 (**Fig. 2A**). Immunoassay values from each of the 8 tests were compared with the measured IC_{50} values (**Fig. 2B**). As expected, strong correlations were observed for all spike-based assays, as determined by the Spearman rank correlation coefficient, with *P* values lower than 0.000002 for all assays other than the nucleocapsid-based Roche test (**Fig. 2C**). These findings correspond with previous studies, which showed that spike-based immunoassays exhibit better correlations with IC_{50} values than the nucleocapsid-based Roche assay (33-35).

While there is a clear relationship between immunoassay values and neutralization efficacies in all comparisons, our primary question concerned the relative balance of these two factors in each assay, requiring a different metric. To better assess the relative abilities of the different capture antigens to estimate neutralization efficacies of the donor samples we used the precision metric. Precision was calculated by the ratio between the number of samples that are positive for neutralization at the selected threshold and the number of samples that are positive for SARS-CoV-2 antibodies by their immunoassay values. The level of precision was determined for subsets of the samples with progressively higher immunoassay thresholds for inclusion; from the 0^{th} percentile (all samples are included in the test) to the 98^{th} percentile (only samples with the top 2% of immunoassay values are included). Specific thresholds for neutralization were tested first, whereby a sample was considered neutralization-positive if the IC_{50} value was greater than a dilution of 1:500 or 1:2,000 (**Fig. 3A**). As expected, the use of samples from higher immunoassay percentiles resulted in higher precision. Differences between the immunoassays were more pronounced when the high neutralization threshold (1:2,000) was set. At this threshold, precision of the nucleocapsid-based Roche assay was low. Surprisingly, the cbELISA, which measures binding of antibodies to the native membrane-associated form of spike, also exhibited lower precision than other spike-based assays.

Given that performance of the assays can vary at each neutralization threshold, we sought to generate a metric that would describe performance across a range of neutralization thresholds. To this end, we first calculated for each threshold (from 1:500 to 1:2,500) the minimal immunoassay percentile required to achieve a precision level of 0.9 (see boundary line for Ecto ELISA as example in **Fig. 3B** and all assays in **Supp. Fig. S4**). The area above the boundary line indicates the percentile-threshold combinations that yield a precision of 0.9 or higher, which allows us to compare overall performance characteristics between immunoassays; the greater the area, the higher the ability of the assay to predict neutralization

across all IC_{50} thresholds. The highest performance was observed for the Ortho, Liaison, Ecto and RBD assays, followed by NTD, TrimericS and cbELISA (**Fig. 3C**). Since the Roche assay did not achieve a precision of 0.9, the areas above the curve could not be computed. We then calculated the area above the curve when the required precision was set at levels ranging between 0.75 and 0.95. For most precision requirement levels in this range, the lowest performance was observed for the Roche assay, followed by cELISA, with modestly better performance for the TrimericS and NTD (**Fig. 3D**). All other assays exhibited similar performance across the different precision requirements. To determine statistical significance of the differences between performance of any two assays, we performed a permutation-based test (see Materials and Methods section). Briefly, for each pair of assays compared, we measured the area above the curve and calculated the difference. We then permuted for each patient sample the immunoassay identifiers, the area above the curve was recalculated for both immunoassays and the difference determined. The fraction of the times the difference was greater using the permuted values relative to the unpermuted values was calculated as the *P* value. Significant differences for a one-sided test (*P* values lower than 0.05) were observed between the cbELISA and all other spike-based assays. The NTD and TrimericS assays showed moderate differences from other assays; however, they were not significant at the 95% confidence level (**Fig. 3E**). Therefore, the ability of cbELISA (i.e., the full-length membrane-bound form of spike) to predict neutralization was significantly lower than that of all other assays that apply isolated domains of the protein as capture antigens.

To independently validate the above findings, we also measured neutralization titers for 24 of the serum samples using infectious SARS-CoV-2 under BSL-3 conditions, and correlated those findings with immunoassays values. Virus-induced cytopathology was used to detect infection. The dilution of serum at which cytopathic effects were observed in fewer than 50% of the wells was determined, and data were fit to a regression model to calculate the precise IC_{50}

value. For three of the samples, the IC_{50} was not achieved at the lowest dilution of the serum used (1:40); the remainder showed a range of IC_{50} values, with a median dilution of 1:212 (**Fig. 4A**). A strong correlation was observed between the neutralization titers of the sera measured using the replicative SARS-CoV-2 and the VSV-based pseudovirus that contains the spike protein (**Fig. 4B**). As expected, IC_{50} values in the pseudovirus assay were higher than those measured using infectious virus, since the former measures the dilution at which 50% of virus infectivity is reduced whereas the latter assay measures the dilution at which more than 50% of wells show complete neutralization of all input virus.

We compared immunoassay values of the samples with their neutralization efficacies of replicative SARS-CoV-2 (**Fig. 4C**). Strong correlations were observed for all spike-based assays (**Supp. Fig. S5**). Precision analyses using an IC_{50} threshold of 1:400 demonstrated considerable differences between performance of the assays (**Fig. 4D**). Comparison of the overall performance of the immunoassays across neutralization thresholds of 1:50 to 1:500 (using the area above the curve metric with a required precision of 0.9) showed a similar pattern to the pseudovirus-based measurements (compare **Fig. 4E** and **Fig. 3C**); the poorest performance was observed for the Roche assay, followed by NTD and cbELISA. All other assays performed similarly well. Comparison of assay performance at precision levels of 0.75-0.95 showed modest differences between cbELISA or NTD and all other spike-based assays (**Fig. 4F**); however, these differences did not reach a significance level of 0.05 (**Fig. 4G**)

Taken together, these results demonstrate that performance of immunoassays based on RBD, S1, or monomeric and dimeric forms of S1/S2 to estimate the neutralization efficacy of each sample was similar. Modestly lower predictive capacities are observed when NTD and the full-length form of spike (as measured by cbELISA) are used as the capture antigens. Further, comparison of the precision of the immunoassays to predict neutralization using pseudovirions containing SARS-CoV-2 spike or replication-competent viruses yield roughly similar findings.

COVID-19 convalescent samples exhibit a similar level of relative neutralization potency

The above results show that different forms of spike used as capture antigens (NTD, RBD, S1 or Ecto) can estimate neutralization with similar precision. Furthermore, the relationship between the levels of NTD and RBD antibodies is relatively conserved in different individuals; these antibodies compose the vast majority of the antibodies generated against spike. We asked whether the neutralization efficacy increases with higher proportions of RBD- or NTD-targeting antibodies (relative to all spike-targeting antibodies). Comparison of the RBD-to-Ecto or NTD-to-Ecto ratios with the neutralization efficacy of the samples showed no evidence for a relationship between these variables (**Fig. 5A** and **5B**). Similarly, the RBD-to-NTD ratio was not associated with the neutralization efficiency of the samples (**Fig. 5C**). These findings indicate that convalescent samples with high neutralizing activity do not contain a higher proportion of antibodies that target the RBD or NTD.

A large proportion of spike-targeting antibodies elicited by infection are non-neutralizing (36, 37). A recent study has shown that infected and immunized hosts with high levels of spike-specific antibodies generate a significantly higher proportion of non-neutralizing antibodies than individuals with lower levels of anti-spike antibodies (38). To explore this relationship in our samples, we implemented a model to examine evidence for a variable ratio between immunoassay values and neutralization efficacy. Two computational approaches were used; the first looks for non-log-linearity in the relationship between neutralization and immunoassay tests, whereas the second considers their rank-ratios and examines evidence for a systematic change over the ranks of the immunoassay results.

To compare the variables and avoid a bias related to the dynamic ranges of the values, we corrected the $\log_{10}$-transformed immunoassay and neutralization IC_{50} values to the same

scale by adjustment to a range from 0.1 to 1. For each sample we calculated the ratio between the immunoassay value and the IC_{50} value (see analysis of the Ecto ELISA data in **Fig. 5D**). This ratio was compared between the 20 samples with the lowest immunoassay values and the 20 samples with the highest immunoassay values. Evaluation of these results did not find significantly different ratios in the two groups (see *P* value for an unpaired T test in **Fig. 5D**). A similar lack of a significant difference was observed when the RBD and NTD were used as capture antigens (**Supp. Fig. S6**). However, the cbELISA results suggested a higher ratio (i.e., a lower relative neutralization efficacy) for the samples with high antibody levels.

To further explore whether the immunoassay-to-neutralization ratio shows any indication of dependence on the immunoassay value, we examined the variability in this ratio by looking for non-linearity in their log-relationship using all 85 samples. The null hypothesis tested was that the log-scale relationship between these variables should be linear, which was tested by considering a quadratic term for immunoassay results in a multiple linear regression (MLR) model. While the data appeared well modelled directly on a log-10 scale, to eliminate concerns about distributional assumptions, the regression coefficient was bootstrapped, and the corresponding 95% confidence interval determined. We first analyzed the results of the Ecto assay. As shown in **Fig. 5E**, an MLR slope value of 0 (i.e., lack of a quadratic effect, leaving a linear increase in neutralization activity for a given increase in binding) lies within the 95% confidence interval, so we fail to reject the null hypothesis that the variables follow a ratio relationship. Similar analyses of the data from the NTD, RBD and cbELISA tests also failed to show evidence at the 95% level to support a non-linear relationship between immunoassay values and neutralization (**Fig. 5F**).

We also applied a rank-based approach, whereby immunoassay and neutralization values were transformed to their ranks (from 1 to 85). A simple linear regression (SLR) coefficient was then fitted to the relationship between the immunoassay rank value and

immunoassay-to-neutralization rank-ratio, and bootstrapping was applied once more to produce 95% confidence intervals. The null hypothesis tested was that a slope of zero exists for this relationship. Again, no evidence was observed to support the notion that the ratio between Ecto values and neutralization varies across different levels of S1/S2-targeting antibodies (**Fig. 5G**). A similar bootstrapping analysis of the rank values for the RBD, NTD and cbELISA failed to demonstrate a non-zero slope that would indicate a linear relationship between the two variables (**Fig. 5H**).

Given the sample size (n=85), the presence of a strong relationship between neutralization fraction and antibody binding activity seems unlikely. Nevertheless, we do observe negative non-significant coefficients for the quadratic effect of log-binding activity on neutralization levels, and positive non-significant coefficients of for the linear relationship between binding activity and the rank ratio of binding to neutralization (**Fig. 5, G** and **H**). Both of these results indicate the plausibility of a weak relationship between the neutralization ratio and binding activity measures, in which higher binding activity could be associated with lower proportional neutralization activity, but the magnitude of such an effect is likely to be limited.

DISCUSSION

Over the course of the COVID-19 pandemic, our understanding of the antibody response against SARS-CoV-2 has evolved. Initial investigations suggested that most neutralizing antibodies elicited by infection or vaccination target the RBD (9, 39). More recent studies have shown a co-dominance of antibodies that target the RBD and NTD (25, 26). Proteomic deconvolution studies of the IgG repertoire in COVID-19 convalescent patients suggested that the bulk of the neutralizing response targets epitopes outside the RBD (40). To better understand the target specificity of the response in different individuals, we analyzed the relative

level of antibodies against different domains, subunits and oligomeric forms of spike in COVID-19 convalescent samples. Our findings suggest the model shown in **Fig. 6**. A polyclonal antibody response is elicited in each infected individual against multiple domains of spike. High variation is observed between individuals in the amounts of antibodies generated; however, there is limited variation in the proportion of antibodies against the RBD and NTD (relative to all anti-spike antibodies). Similarly, limited variation is observed in the relationship between the amounts of antibodies against the RBD and NTD, with a ratio ranging between 1 and 3 in 78% of subjects. Importantly, the relative potency of the response (i.e., the level of neutralizing activity relative to the level of antibodies generated) is also constant in different individuals. Thus, the domain specificity and relative inhibitory activity of the response is conserved among individuals, with the main variation being the total amount of the antibodies produced.

Multiple commercial immunoassays have been developed that apply different components of the spike protein as the capture antigen (35, 41-44). Spike-based assays have been shown to estimate well the neutralization efficacy of convalescent serum and plasma samples (27-30). They are thus applied as qualitative measures of immunization status and can potentially serve as indirect measures of the efficacy of the anti-SARS-CoV-2 humoral response. Our studies suggest that any soluble form of spike that contains the RBD or NTD can serve as a capture antigen to accurately determine the immunization status of the individual and potentially the efficacy of the anti-SARS-CoV-2 humoral response. The constant proportion of antibodies against different spike domains also explains the ability of immunoassays that use various forms of the protein as capture antigens to predict neutralization. Indeed, our findings suggest that determinations of neutralizing titers based on serological tests do not require native forms of the protein as the capture antigen; RBD exhibits a similar predictive capacity to that of S1 or S1/S2, with only modestly lower performance for NTD. Thus, inclusion of S2 or trimerization of the protein to mimic the native form of spike does not improve the ability to

358 estimate the amount of neutralizing antibodies. In fact, the poorest performance was observed
359 for the full-length, membrane-bound form of the protein measured by cell-based ELISA. The
360 lower predictive capacity of the cbELISA may result from detection of non-neutralizing
361 antibodies that may recognize the native form of spike (37). Alternatively, differential post-
362 translational processing of spike in the HOS cells (relative to the human embryonic kidney 293T
363 cells used to produce the recombinant proteins for these assays) may affect antigenicity of this
364 protein (45).

365 We were surprised to discover that subjects with different amounts of spike-specific
366 antibodies contained a constant level of relative potency. Such results contrast with a recent
367 study by Amanat et al., which suggested that convalescent samples that contain high amounts
368 of spike antibodies (as measured by the Mount Sinai Laboratory COVID-19 ELISA IgG Antibody
369 Test) contain a higher proportion of non-neutralizing antibodies that target the full-length
370 ectodomain of spike (38). It should be noted that in their calculations, the authors analyzed the
371 immunoassay-to-IC_{50} ratios using the raw values obtained in these tests. Unfortunately, such an
372 approach can introduce a bias if the dynamic ranges of the two variables differ, which may
373 impact the results of the analysis. To address this potential bias, we performed our calculations
374 using ranks and values that were corrected to the same scale. Both approaches showed similar
375 results, whereby the relative potency is constant in different samples, regardless of the amount
376 of anti-spike antibodies generated. Future studies will reveal whether the target specificity of
377 antibodies with neutralizing activity is also constant in different individuals and independent of
378 the robustness of the response. Such studies are of particular importance in vaccinated
379 individuals, to accurately quantify and characterize specificity of the antibody fractions that can
380 protect from infection.

381

MATERIALS AND METHODS

Collection of plasma and serum from donors and patients

All blood donors were screened following the FDA guidance instructions under an institutional review board approved protocol (IRB #202003554). The consent signed by all donors allowed the use of blood samples for research purposes. Donors were identified and screened following FDA guidelines at the time they enrolled. Two study groups were assessed. The first is composed of 57 convalescent serum samples from subjects that had either been confirmed by reverse transcription polymerase chain reaction (RT-PCR) to be SARS-CoV-2 positive from a nasopharyngeal swab (n=51) or had signs or symptoms of COVID-19 and were found to be positive by serological testing (n=6). All donors except one had relatively mild COVID-19 symptoms; this donor was hospitalized for one day due to palpitations. Donor screening was performed at least 10 days after resolution of symptoms. At the time of plasma collection, serum samples were collected in serum separator tubes and allowed to clot for at least 30 minutes. Serum was then isolated, aliquoted and stored at -80°C until use. The second study group is composed of convalescent plasma collected from women hospitalized for delivery, who had previously been infected by SARS-CoV-2, as confirmed by a SARS-CoV-2-positive PCR (n=7) or positive serology test (n=21). Samples were collected in EDTA-containing tubes, aliquoted and frozen until use at -80°C.

Cells lines

Vero-E6 cells, human embryonic kidney (HEK) 293T cells and human osteosarcoma (HOS) cells were obtained from the American Type Culture Collection (ATCC). Cells were cultured in Dulbecco's modified Eagle medium (DMEM) supplemented with 2-10% fetal calf serum (FCS) and 1% penicillin/streptomycin. All cells were maintained in a humidified incubator

406 at 37°C and 5% CO_2.

407

408 **Recombinant proteins and their production**

409 Capture antigens that contain different spike protein components were generated. The
410 NTD, RBD or ectodomain of S1/S2 (Ecto) antigens were fused to the Fc region of human IgG1,
411 rendering them dimeric. NTD and RBD contain amino acids 1-309 and 310-529 of spike,
412 respectively. The Ecto protein contains the entire ectodomain of spike (amino acids 1-1274). To
413 abrogate the furin cleavage site in Ecto, we substituted the Arg-Arg-Ala-Arg motif at position
414 683-686 with Ser-Ser-Ala-Ser. All proteins were produced by transient transfection of 293T cells
415 using polyethyleneimine (PEI), as previously described (46). Proteins were harvested in 293S
416 ProCDM and purified using Protein A beads. Eluted products were dialyzed against phosphate
417 buffered saline (pH 7.4). All proteins were analyzed by SDS-PAGE and visualized by silver
418 staining to verify their molecular weight and purity.

419

420 **ELISA using RBD, NTD and S1/S2 as capture antigens**

421 The RBD, NTD and Ecto recombinant proteins were used as capture antigens in an
422 enzyme-linked immunosorbent assay (ELISA). Briefly, proteins were suspended in PBS at a
423 concentration of 25 nM (2 µg/mL of NTD, 1.37 µg/mL of RBD and 5 µg/mL of Ecto) and
424 incubated overnight in protein-binding 96-well plates (PerkinElmer). The next day, wells were
425 washed once with blocking buffer, composed of 140 mM NaCl, 1.8 mM $CaCl_2$, 1 mM $MgCl_2$, 25
426 mM Tris pH 7.5, 20 mg/ml BSA and 1.1% nonfat dry milk. Serum or plasma samples were
427 diluted 1:500 (vol:vol) in blocking buffer, added to the wells and incubated for 45 min at room
428 temperature. Samples were then washed four times with blocking buffer and a horseradish
429 peroxidase (HRP)-conjugated secondary antibody that targets the kappa light chain of human

IgG1 was added (diluted 1:1200 in blocking buffer). After incubation for one hour at room temperature, samples were washed 5 times with blocking buffer and 5 times with washing buffer (140 mM NaCl, 1.8 mM $CaCl_2$, 1 mM $MgCl_2$ and 25 mM Tris pH 7.5). HRP enzyme activity was measured by light emission using Supersignal West Pico Plus chemiluminescence detection reagents with a Synergy H1 microplate reader.

Cell-based ELISA measurements of antibodies against SARS-CoV-2 spike

Binding of serum antibodies to SARS-CoV-2 spike expressed on HOS cells was measured using a previously-described cell-based ELISA system (22, 24). Briefly, HOS cells were seeded in white opaque 96-well plates (1.4×10^4 cells per well) and transfected the next day with 80 ng per well of pCG1-SARS-2-S plasmid expressing SARS-CoV-2 spike using JetPrime transfection reagent. To quantify background binding of the antibodies to the cells, a similar number of wells was transfected using a negative control plasmid (ΔKS) that does not encode for a viral protein product (23). Three days after transfection, cells were washed with blocking buffer, and serum samples diluted 1,000-fold in blocking buffer were incubated with the cells for one hour at room temperature. Cells were then washed 5 times with blocking buffer and incubated for 45 minutes at room temperature with an HRP-conjugated goat anti-human kappa chain preparation that was diluted 1:1,200 in blocking buffer. Cells were then washed 5 times with blocking buffer and 5 times with washing buffer. HRP enzyme activity was measured by chemiluminescence with a Synergy H1 microplate reader.

Commercial immunoassays to measure antibodies that target SARS-CoV-2 proteins

The DiaSorin Liaison SARS-CoV-2 S1/S2 IgG chemiluminescence assay detects IgG against spike subunits S1 and S2. Samples were analyzed according to the manufacturer's

guidelines on a DiaSorin Liaison XL automated chemiluminescence analyzer (DiaSorin, Saluggia, Italy). A signal of 15 arbitrary units (AU) per mL or higher is defined by the manufacturer as a positive result. The DiaSorin TrimericS IgG assay applies the soluble trimeric form of the S1/S2 subunits. Samples were analyzed on a DiaSorin Liaison XL automated chemiluminescence analyzer. A signal of 13 AU/mL is defined as a positive result. The Roche electrochemiluminescence immunoassay measures total immunoglobulins that target the SARS-CoV-2 nucleocapsid (N) protein. Samples were analyzed according to the manufacturer's guidelines using the Elecsys Anti-SARS-CoV-2 assay on the Roche cobas e602 platform (Roche Diagnostics). A cut-off index (COI) of 1.0 or higher is defined by the manufacturer as a positive result. The Ortho COVID-19 IgG antibody test was performed on Ortho's VITROS® system. The signal at cutoff (S/C) value as defined by the manufacturer is 1 unit or greater for a reactive sample. For simplicity, all values of the commercial immunoassays are reported in arbitrary units (AUs).

Infection and neutralization of replication-competent SARS-CoV-2

SARS-CoV-2 strain USA-WA1_2020 was obtained from BEI Resources and maintained under biosafety level 3 (BSL-3) conditions. To propagate virus, Vero-E6 cells cultured in DMEM/FCS 2% were infected at a multiplicity of infection (MOI) of 0.001. Forty-eight hours after infection, supernatants were harvested, filtered through 0.45 µm pore-sized membranes, and frozen at -80°C until use. To quantify the amount of infectious virus, Vero-E6 cells were seeded in 96-well plates (1.5×10^4 cells per well). The next day, serial dilutions of the virus were added to 8 replicate wells for each dilution and cytopathic effects were evaluated over the next 5 days. The median tissue culture infectious dose ($TCID_{50}$) was used to quantify virus titer, which describes the dilution of the virus at which fewer than half of the replicate wells show cytopathic effects.

To measure neutralization, serial two-fold dilutions of the serum samples (ranging from 1:40 to 1:2,560) were prepared in DMEM/FCS 2%. Virus was added to the diluted serum at a final concentration of 25 $TCID_{50}$ per well. Samples were incubated at room temperature for one hour and added to Vero-E6 cells seeded the day before in 96-well plates (1.5×10^4 cells per well). Six replicate wells were used for each dilution. Cells were then cultured for 4 days at 37°C until infectivity was evaluated. The number of wells in which intact monolayers were present was assessed using an inverted light microscope. The 50% neutralizing titer (IC_{50}) was calculated by the serum dilution at which 50% or more of the wells showed no cytopathic effects. To determine the precise IC_{50} value, the number of wells in which cytopathic effects were observed at each serum dilution was recorded. These values, along with the log-transformed dilution values were fit to a non-linear regression model using GraphPad Prism 8 to calculate the IC_{50} value.

Production and neutralization of vesicular stomatitis virus pseudotyped by the SARS-CoV-2 spike protein

Vesicular stomatitis virus (VSV) pseudovirions bearing the SARS-CoV-2 spike protein (VSV-SARS2-S) were generated as previously described (5). Briefly, 293T cells were seeded in 100 mm plates (2.2×10^6 cells per plate) and transfected 24 hours later by 16 µg of pCG1-SARS-2-S plasmid (a kind gift from Dr. Stefan Pöhlmann) using PEI transfection protocol (46). Twenty-four hours after transfection, cells were infected with a stock of VSV pseudovirus that encodes the firefly luciferase gene in place of the native VSV-G glycoprotein gene and contains the glycoprotein of Lassa virus (5). Six hours later, infected cultures were washed twice with phosphate buffered saline (PBS, pH 7.4) to remove input pseudovirions, and fresh DMEM/FCS 2% was added. Media was collected at 24- and 48-hours after infection, the supernatants were filtered through 0.45 µm pore-sized membranes and centrifuged at 5,380 × g for 16 hours at

4°C. The pellet was resuspended in PBS and centrifuged through a 20% sucrose cushion at 134,000 × g for 2 hours at 10°C. Pellets containing the pseudoviruses were resuspended in PBS and stored at -80°C until use.

For neutralization assays, two-fold serial dilutions of the serum samples were prepared in DMEM/5% FCS, ranging between 1:40 and 1:2,560. Viruses were added to the diluted serum at a concentration calculated to yield between 100,000 and 200,000 relative light units (RLUs) of luciferase activity per well. These values were determined to be within the linear range of virus input versus luciferase activity measured. Vero-E6 target cells were seeded the day before infection in 96-well white opaque flat-bottomed plates (1.5×10^4 cells per well). The virus-serum or virus-plasma mixture was incubated for one hour at 37°C and added to the wells. Six replicate wells were used for each condition. Samples were then incubated for 24 h at 37°C, after which the media were removed and 35 µl of Passive Lysis buffer (Promega) was added to each well. Luciferase activity was recorded as a measure of viral infection, as previously described (24). Briefly, 100 µl of luciferin buffer containing 15 mM $MgSO_4$, 15 mM KPO_4 (pH 7.8), 1 mM ATP, and 1 mM dithiothreitol was added to each well, followed by 50 µl of 1 mM d-luciferin potassium salt (Syd Laboratories). Luminescence was detected using a Synergy H1 Hybrid reader (BioTek Instruments).

Permutation test to compare precision of immunoassays

For each immunoassay, we obtained the curve that describes the required percentile of samples for each neutralization threshold to yield a precision of 0.9. The area above the curve was then determined, which describes all percentile-neutralization threshold combinations that yield a precision level higher than the minimum precision of interest (here, 0.9). This metric thus captures the precision of each assay across multiple neutralization thresholds. To test for

significant difference between the area above the curve for any two immunoassays, we used a permutation test. The null and alternative hypotheses for a one-sided test can be stated as:

$$H_0: A_i = A_j$$

$$H_1: A_i > A_j \qquad i \neq j \ \ \& \ \ i, j = 1, 2, \dots, M$$

where A_i and A_j describe the area above the curve for immunoassays i, and j, respectively, and M is the total number of immunoassays tested. To test the above hypothesis, we first log-transformed immunoassay values and standardized them to a scale of 0 to 1:

$$X^i_{new} = \frac{X^i - \min(X^i)}{\max(X^i) - \min\,(X^i)}$$

where, X^i is the vector of values for immunoassay i. The difference between the area above the curve for i and j was then calculated, denoted as D_{ij}. We then performed a permutation test whereby we permuted for each patient sample the immunoassay identifiers and the area above the curve was recalculated for each immunoassay. This process was repeated 1,000 times ($k = 1, 2, \dots, 1000$). The difference between the areas above the curves for each iteration of the permutation test was defined as d^k_{ij}. The instances that the permuted value of d^k_{ij} was greater than or equal to the non-permuted D_{ij} was calculated and expressed as a fraction of the number of iterations performed, which was defined as the *P* value for testing the null hypothesis.

Multiple linear Regression and rank-based simple linear regression

In the absence of a universal gold standard, $\log_{10}$-transformations appeared reasonable to capture immunoassay values and neutralization activity. Under our null hypothesis, a change in binding activity, $\log_{10}(X)$, should be associated with a linear increase in neutralization, $\log_{10}(Y)$. This relationship can be expressed as a linear regression on the log-scale:

549 $\log(y) = \beta_0 + \beta_1 \log(x) + \epsilon$. A simple way of detecting departures from this model is to look for
550 curvature in the effect of $\log(x)$: $\log(y) = \beta_0 + \beta_1 \log(x) + \beta_2 \log(x)^2 + \epsilon$. Any evidence that β_2
551 is nonzero will show departure from the hypothesized relationship; for example, if higher values
552 of binding activity produce a diminished change in neutralization efficacy, we would expect β_2 to
553 be negative. We therefore fit a multiple linear regression with the outcome variable of log-IC_{50}
554 and each of the log-scale immunoassay variables in turn as X. To avoid any problematic
555 assumptions about the distribution of the error term ϵ, the MLR was fit under a bootstrapping
556 procedure, in which 50,000 repeated samples were taken to produce a bootstrap distribution of
557 the parameter estimates. This was used to compute non-parametric 95% confidence intervals
558 for the β_2 quadratic effects.

559 In addition to this MLR approach using log-transformed assay values, we conducted a
560 series of rank-based analyses. Rather than focusing on the ratio-relationship directly, we
561 hypothesized that high neutralization values (relative to the sampling distribution) should
562 correspond to high binding values (relative to the sampling distribution), in such a way that the
563 rank-ratios, $\frac{X_r}{Y_r}$, should follow a distribution with mean not depending on the binding rank, X_r.
564 This was investigated via a bootstrapped simple linear regression with the rank-ratio of binding
565 to neutralization as the outcome, and the binding rank as the single explanatory variable. Under
566 the null hypothesis, the slope parameter for the binding rank, β_1, should be equal to zero. We
567 again performed 50,000 repeated samples to produce bootstrap distributions and corresponding
568 non-parametric confidence intervals for β_1.

569

ACKNOWLEDGEMENTS

We thank all blood donors that contributed samples to this study and Julie Kurt from the Department of Pathology and Drs. Mary Rysavy and Kim Kenne from the Department of Gynecology and Obstetrics at the University of Iowa for assistance in coordinating these studies. We also thank Michelle Sexton of the Iowa State Hygienic Laboratory and Dr. Louis Katz of the Mississippi Valley Regional Blood Center for assistance in conducting the immunoassays. This work was supported by the Department of Pathology at the University of Iowa. DWB was supported by NIH T32 AI007511. KR and HVE were supported by NIH T32GM007337. HVE and NR were supported by NIH R01AI134733 and R21 AI144215 to WJM. The funders had no role in study design, data collection and interpretation, or the decision to submit the work for publication. All corresponding authors had full access to all the data in the study and had final responsibility for the decision to submit the manuscript for publication.

Table 1. Immunoassays and capture antigens used in this study.

Assay	Samples tested (serum, plasma)	Capture antigen used in assay	Assay type	Ig isotype detected [a]
NTD (ELISA)	85 (57, 28)	NTD	In-house ELISA	IgG, IgM, IgA
RBD (ELISA)	85 (57, 28)	RBD	In-house ELISA	IgG, IgM, IgA
S1/S2 (ELISA)	85 (57, 28)	S1/S2 ectodomain	In-house ELISA	IgG, IgM, IgA
Cell-based ELISA	85 (57, 28)	Full-length S1/S2 trimers	In-house ELISA	IgG, IgM, IgA
TrimericS (DiaSorin)	85 (57, 28)	Trimeric S1/S2 ectodomain	Commercial assay	IgG
Liaison (DiaSorin)	85 (57, 28)	S1/S2 ectodomain	Commercial assay	IgG
Vitros (Ortho)	60 (57, -)	S1	Commercial assay	IgG
Roche	71 (43, 28)	Nucleocapsid	Commercial assay	IgG, IgM, IgA

[a] The secondary antibody used in the NTD, RBD and Ecto ELISAs and the cell-based ELISA targets the human kappa light chain.

582

583 **FIGURE LEGENDS**

584 **Figure 1.** Comparison of immunoassays that apply different components of the SARS-CoV-2
585 spike protein as capture antigens. **(A)** Top, domains of the spike protein. NTD, N-terminal
586 domain; RBD, receptor-binding domain; CTD, C-terminal domain; TM, transmembrane domain;
587 CT, cytoplasmic tail. Bottom, schematic of the constructs used as capture antigens in this study.
588 **(B)** SARS-CoV-2 antibody levels in 85 convalescent serum and plasma samples were tested
589 using the RBD, NTD and Ecto ELISAs, as well as the cell-based ELISA. Distributions of the
590 $\log_{10}$-transformed values are shown (see similar plots for commercial assays in **Supp. Fig.**
591 **S1C**). **(C)** Spearman rank correlation coefficients between values measured in the eight
592 immunoassays. Cells are colored by the *P* values determined in a two-tailed test. **(D)**
593 Correlation between values in ELISAs that apply the NTD and RBD as capture antigens. RLU,
594 relative light units. **(E)** Correlation between the sum of the values measured in the ELISAs that
595 apply RBD and NTD, and values measured in the ELISA that applies Ecto as the capture
596 antigen. The dashed red line describes a 1:1 relationship. **(F)** Distribution among the 85
597 convalescent samples of the ratio between log-transformed values measured in the RBD and
598 NTD assays.

599

600 **Figure 2.** Relationships between immunoassay values of COVID-19 convalescent samples and
601 their neutralization of spike-containing pseudovirus. **(A)** Neutralization titers of the serum or
602 plasma samples were measured using replication-defective pseudovirus that contains the spike
603 protein of SARS-CoV-2. Data describe the distribution of the $\log_{10}$-transformed IC_{50} values. **(B)**
604 Comparison of neutralization and immunoassay values. All 85 samples are ordered by their
605 neutralization titers (color-coded in shades of pink, with low values in lighter shades). Values
606 measured in immunoassays are color-coded in shades of green. **(C)** Correlations between

607 immunoassay values and neutralization titers. r_S, Spearman correlation coefficient. *P* value, two-
608 tailed test.
609
610 **Figure 3.** Precision of immunoassays to estimate the neutralization efficacy of COVID-19
611 convalescent serum and plasma. **(A)** Calculations of precision across different immunoassay
612 percentiles. Precision was calculated as the number of samples with an IC_{50} greater than the
613 defined threshold relative to the number of samples in the immunoassay percentile tested. Each
614 data point describes precision of an immunoassay to predict neutralization at the indicated IC_{50}
615 threshold using the indicated percentile of samples. **(B)** The area above the curve metric. The
616 border between the shaded and unshaded areas describes the percentiles of Ecto values
617 required to predict neutralization at the indicated thresholds with a precision of 0.9. For
618 example, the intersection between the red lines indicates that, to predict with a precision of 0.9
619 for a threshold IC_{50} of 1:1,000, samples with Ecto values in the 85^{th} percentile should be used.
620 The shaded area describes all neutralization threshold-percentile combinations that yield a
621 precision of 0.9 or higher. **(C)** The area above the curve shown in panel B calculated for all
622 immunoassays, based on a required precision of 0.9. **(D)** Calculations of the area above the
623 curve for required precision levels of 0.75 to 0.95. **(E)** Statistical significance of the differences
624 between predictive capacity of the immunoassays. The area above the curve was calculated for
625 all immunoassays for a precision of 0.9. Significance of the difference between predictive
626 capacity of any two assays was determined by a permutation test. *P* values of the one-sided
627 test are shown. Cells are color coded by the *P* values calculated.
628
629 **Figure 4.** Immunoassay-based estimations of replicative SARS-CoV-2 neutralization. **(A)**
630 Twenty-four serum samples were tested for their neutralization of replicative SARS-CoV-2. The
631 distribution of IC_{50} values is shown. For three samples, the IC_{50} was not achieved at the lowest

dilution (1:40) of the serum (columns colored in red). **(B)** Correlation between IC_{50} values of the 24 serum samples, as measured using replication-competent SARS-CoV-2 and the VSV-SARS-S pseudovirus. **(C)** Comparison of neutralization and immunoassay values. Samples are ordered by their neutralization efficacy of replicative SARS-CoV-2 (color-coded in shades of pink, with low values in lighter shades). Values measured in immunoassays are color-coded in shades of green. **(D)** Precision of immunoassays to estimate SARS-CoV-2 neutralization at an IC_{50} threshold of 1:400 using different percentiles of the samples based on their immunoassay values. **(E)** Area above the curve calculated for a required precision of 0.9. **(F)** Performance of immunoassays to estimate neutralization at precision levels of 0.75 to 0.95. **(G)** Statistical significance of the differences between predictive capacities of the immunoassays, as determined by a permutation test. Calculations apply the area above the curve computed for a required precision of 0.9. *P* values of the one-sided test are shown. Cells are color coded by the *P* values.

Figure 5. Relationship between the relative neutralizing potency of convalescent samples and their content of spike-specific antibodies. **(A,B)** Comparison of the relative RBD or NTD binding values (expressed as a fraction of the Ecto value) and neutralization efficacy of the samples. **(C)** Comparison of the ratio between RBD and NTD values and neutralization efficacy. **(D)** IC_{50} values of convalescent samples and their immunoassay values were log_{10}-transformed and adjusted to a scale of 0.1 to 1. The ratio between the Ecto ELISA value and the IC_{50} of each sample was calculated for all samples. Patient samples are arranged by increasing Ecto values, from left to right. The ratios calculated for the 20 samples with the lowest and the 20 samples with the highest Ecto values were compared using an unpaired T test; the *P* value for a two-tailed test is indicated. **(E)** Bootstrap distribution for quadratic term in MLR describing the relationship between log-Ecto values and log-IC_{50} values, evaluating evidence for a non-

constant ratio relationship. A 95% bootsrap confidence interval was determined from bootstrap sample quantiles. **(F)** The quadratic term was calculated by 50,000 iterations of bootstrap resampling for NTD, RBD, Ecto and cbELISA data. The boxed area shows the second and third quartiles. Whiskers describe the range for two standard deviations. **(G)** Bootstrapped rank regression. The rank order of Ecto values for all 85 samples was determined as well as the ratio between the ranks of the Ecto value and IC_{50}. A simple linear regression model was fit to the relationship between the two variables. A bootstrapping procedure was performed to estimate the slope coefficient. The bootstrap distribution and corresponding 95% confidence interval are shown. **(H)** The rank regression coefficient was calculated by bootstrap resampling using NTD, RBD, Ecto or cbELISA data.

Figure 6. Model of the polyclonal antibody response elicited against the SARS-CoV-2 spike protein. SARS-CoV-2-infected individuals generate different amounts of spike-targeting antibodies (represented by the size of the blue rectangles). The fraction of antibodies that target the RBD or NTD is constant in different individuals, with a mean RBD-to-NTD ratio of 1.8. The relative neutralization potency (represented by the green-shaded area) is also similar in different individuals. Question marks indicate the yet unknown domain distribution of the fraction of antibodies that contains neutralizing activity (i.e., positioning of the green-shaded area).

675 **SUPPLEMENTAL FILES**

676 **Supplemental Figure S1.** Measurements of spike-targeting antibodies in 85 convalescent
677 samples using immunoassays that apply different components of SARS-CoV-2 as capture
678 antigens. **(A)** Distribution of the time interval between the PCR test indicating infection by
679 SARS-CoV-2 and collection time of the samples used for this study. **(B)** Normality tests of
680 immunoassay values. The Shapiro-Wilk test was performed for the immunoassay values and for
681 the log_{10}-transformed immunoassay values. The null hypothesis for this test is that the data are
682 normally distributed. *P* values lower than 0.05 indicate that the null hypothesis is rejected. **(C)**
683 Distribution of immunoassay values measured for 85 convalescent using commercial tests.

684

685 **Supplemental Figure S2.** Comparison of the log_{10}-transformed values measured in eight
686 immunoassays for 85 convalescent serum and plasma samples. Values in the commercial
687 assays are expressed in arbitrary units (AUs) whereas values in ELISAs are expressed in
688 relative light units (RLUs). Values in the x and y axes are shown in log_{10} scale. Correlation
689 coefficients are shown in **Fig. 1C**.

690

691 **Supplemental Figure S3.** Relationship between timing of sample collection and target
692 specificity of the antibody response. The interval (in days) between the PCR-positive test
693 indicating SARS-CoV-2 infection and the time of plasma or serum collection for these studies
694 was determined. **(A-C)** Immunoassay values are compared between samples with an interval of
695 10-45 days (n=43), and samples with an interval of 103-277 days (n=9). **(D,E)** Comparison of
696 the RBD/Ecto or NTD/Ecto ratios for samples collected after the indicated intervals from
697 detection of infection by PCR. *P* Value, two-tailed test.

698

699 **Supplemental Figure S4.** Immunoassay percentiles required to predict neutralization at the
700 indicated thresholds with a precision of 0.9. The shaded area describes the combination
701 between neutralization thresholds and sample immunoassay percentiles that allow prediction
702 with a precision of 0.9 or higher. The Roche test did not achieve a precision of 0.9, and thus a
703 value could not be computed for this assay.
704
705 **Supplemental Figure S5.** Relationships between immunoassay values of COVID-19
706 convalescent samples and their neutralization of replicative SARS-CoV-2. r_S, Spearman
707 correlation coefficient. *P* value, two-tailed test.
708
709 **Supplemental Figure S6.** Relationship between the level of spike-specific antibodies in
710 convalescent samples and their relative neutralization potency. IC_{50} values of convalescent
711 samples and their immunoassay values were log-transformed and adjusted to a scale of 0.1 to
712 1. For each sample, the ratio between the immunoassay value and the IC_{50} value was
713 calculated and shown. Samples are ordered by increasing immunoassay values from left to
714 right. The ratios calculated for the 20 samples with the lowest immunoassay values and the 20
715 samples with the highest immunoassay values were compared using an unpaired T test; the *P*
716 values for a two-tailed test are indicated.
717
718 **Supplemental Table S1.** Sample donor information. n.a., indicated data not available.

719 ## REFERENCES

720 1. Shang B, Wang XY, Yuan JW, Vabret A, Wu XD, Yang RF, Tian L, Ji YY, Deubel V, Sun
721 B. 2005. Characterization and application of monoclonal antibodies against N protein of
722 SARS-coronavirus. Biochem Biophys Res Commun 336:110-7.
723 2. Walls AC, Park YJ, Tortorici MA, Wall A, McGuire AT, Veesler D. 2020. Structure,
724 Function, and Antigenicity of the SARS-CoV-2 Spike Glycoprotein. Cell 181:281-292 e6.
725 3. Hoffmann M, Kleine-Weber H, Pohlmann S. 2020. A Multibasic Cleavage Site in the
726 Spike Protein of SARS-CoV-2 Is Essential for Infection of Human Lung Cells. Mol Cell
727 78:779-784 e5.
728 4. Wrapp D, Wang N, Corbett KS, Goldsmith JA, Hsieh CL, Abiona O, Graham BS,
729 McLellan JS. 2020. Cryo-EM structure of the 2019-nCoV spike in the prefusion
730 conformation. Science 367:1260-1263.
731 5. Hoffmann M, Kleine-Weber H, Schroeder S, Kruger N, Herrler T, Erichsen S, Schiergens
732 TS, Herrler G, Wu NH, Nitsche A, Muller MA, Drosten C, Pohlmann S. 2020. SARS-
733 CoV-2 Cell Entry Depends on ACE2 and TMPRSS2 and Is Blocked by a Clinically
734 Proven Protease Inhibitor. Cell 181:271-280 e8.
735 6. Tang T, Jaimes JA, Bidon MK, Straus MR, Daniel S, Whittaker GR. 2021. Proteolytic
736 Activation of SARS-CoV-2 Spike at the S1/S2 Boundary: Potential Role of Proteases
737 beyond Furin. ACS Infect Dis 7:264-272.
738 7. Cao Y, Su B, Guo X, Sun W, Deng Y, Bao L, Zhu Q, Zhang X, Zheng Y, Geng C, Chai
739 X, He R, Li X, Lv Q, Zhu H, Deng W, Xu Y, Wang Y, Qiao L, Tan Y, Song L, Wang G, Du
740 X, Gao N, Liu J, Xiao J, Su XD, Du Z, Feng Y, Qin C, Qin C, Jin R, Xie XS. 2020. Potent
741 Neutralizing Antibodies against SARS-CoV-2 Identified by High-Throughput Single-Cell
742 Sequencing of Convalescent Patients' B Cells. Cell 182:73-84 e16.

743 8. Wu Y, Wang F, Shen C, Peng W, Li D, Zhao C, Li Z, Li S, Bi Y, Yang Y, Gong Y, Xiao H,
744 Fan Z, Tan S, Wu G, Tan W, Lu X, Fan C, Wang Q, Liu Y, Zhang C, Qi J, Gao GF, Gao
745 F, Liu L. 2020. A noncompeting pair of human neutralizing antibodies block COVID-19
746 virus binding to its receptor ACE2. Science 368:1274-1278.
747 9. Zhou X, Ma F, Xie J, Yuan M, Li Y, Shaabani N, Zhao F, Huang D, Wu NC, Lee CD, Liu
748 H, Li J, Chen Z, Hong Y, Liu WH, Xiao N, Burton DR, Tu H, Li H, Chen X, Teijaro JR,
749 Wilson IA, Xiao C, Huang Z. 2021. Diverse immunoglobulin gene usage and convergent
750 epitope targeting in neutralizing antibody responses to SARS-CoV-2. Cell Rep
751 35:109109.
752 10. Brouwer PJM, Caniels TG, van der Straten K, Snitselaar JL, Aldon Y, Bangaru S, Torres
753 JL, Okba NMA, Claireaux M, Kerster G, Bentlage AEH, van Haaren MM, Guerra D,
754 Burger JA, Schermer EE, Verheul KD, van der Velde N, van der Kooi A, van Schooten J,
755 van Breemen MJ, Bijl TPL, Sliepen K, Aartse A, Derking R, Bontjer I, Kootstra NA,
756 Wiersinga WJ, Vidarsson G, Haagmans BL, Ward AB, de Bree GJ, Sanders RW, van
757 Gils MJ. 2020. Potent neutralizing antibodies from COVID-19 patients define multiple
758 targets of vulnerability. Science 369:643-650.
759 11. Cerutti G, Guo Y, Zhou T, Gorman J, Lee M, Rapp M, Reddem ER, Yu J, Bahna F,
760 Bimela J, Huang Y, Katsamba PS, Liu L, Nair MS, Rawi R, Olia AS, Wang P, Zhang B,
761 Chuang GY, Ho DD, Sheng Z, Kwong PD, Shapiro L. 2021. Potent SARS-CoV-2
762 neutralizing antibodies directed against spike N-terminal domain target a single
763 supersite. Cell Host Microbe 29:819-833 e7.
764 12. Robbiani DF, Gaebler C, Muecksch F, Lorenzi JCC, Wang Z, Cho A, Agudelo M, Barnes
765 CO, Gazumyan A, Finkin S, Hagglof T, Oliveira TY, Viant C, Hurley A, Hoffmann HH,
766 Millard KG, Kost RG, Cipolla M, Gordon K, Bianchini F, Chen ST, Ramos V, Patel R,
767 Dizon J, Shimeliovich I, Mendoza P, Hartweger H, Nogueira L, Pack M, Horowitz J,
768 Schmidt F, Weisblum Y, Michailidis E, Ashbrook AW, Waltari E, Pak JE, Huey-Tubman

KE, Koranda N, Hoffman PR, West AP, Jr., Rice CM, Hatziioannou T, Bjorkman PJ, Bieniasz PD, Caskey M, Nussenzweig MC. 2020. Convergent antibody responses to SARS-CoV-2 in convalescent individuals. Nature 584:437-442.

13. Zhou D, Dejnirattisai W, Supasa P, Liu C, Mentzer AJ, Ginn HM, Zhao Y, Duyvesteyn HME, Tuekprakhon A, Nutalai R, Wang B, Paesen GC, Lopez-Camacho C, Slon-Campos J, Hallis B, Coombes N, Bewley K, Charlton S, Walter TS, Skelly D, Lumley SF, Dold C, Levin R, Dong T, Pollard AJ, Knight JC, Crook D, Lambe T, Clutterbuck E, Bibi S, Flaxman A, Bittaye M, Belij-Rammerstorfer S, Gilbert S, James W, Carroll MW, Klenerman P, Barnes E, Dunachie SJ, Fry EE, Mongkolsapaya J, Ren J, Stuart DI, Screaton GR. 2021. Evidence of escape of SARS-CoV-2 variant B.1.351 from natural and vaccine-induced sera. Cell 184:2348-2361 e6.

14. Zost SJ, Gilchuk P, Chen RE, Case JB, Reidy JX, Trivette A, Nargi RS, Sutton RE, Suryadevara N, Chen EC, Binshtein E, Shrihari S, Ostrowski M, Chu HY, Didier JE, MacRenaris KW, Jones T, Day S, Myers L, Eun-Hyung Lee F, Nguyen DC, Sanz I, Martinez DR, Rothlauf PW, Bloyet LM, Whelan SPJ, Baric RS, Thackray LB, Diamond MS, Carnahan RH, Crowe JE, Jr. 2020. Rapid isolation and profiling of a diverse panel of human monoclonal antibodies targeting the SARS-CoV-2 spike protein. Nat Med 26:1422-1427.

15. Dogan M, Kozhaya L, Placek L, Gunter C, Yigit M, Hardy R, Plassmeyer M, Coatney P, Lillard K, Bukhari Z, Kleinberg M, Hayes C, Arditi M, Klapper E, Merin N, Liang BT, Gupta R, Alpan O, Unutmaz D. 2021. SARS-CoV-2 specific antibody and neutralization assays reveal the wide range of the humoral immune response to virus. Commun Biol 4:129.

16. Chi X, Yan R, Zhang J, Zhang G, Zhang Y, Hao M, Zhang Z, Fan P, Dong Y, Yang Y, Chen Z, Guo Y, Zhang J, Li Y, Song X, Chen Y, Xia L, Fu L, Hou L, Xu J, Yu C, Li J,

794 Zhou Q, Chen W. 2020. A neutralizing human antibody binds to the N-terminal domain
795 of the Spike protein of SARS-CoV-2. Science 369:650-655.
796 17. Suryadevara N, Shrihari S, Gilchuk P, VanBlargan LA, Binshtein E, Zost SJ, Nargi RS,
797 Sutton RE, Winkler ES, Chen EC, Fouch ME, Davidson E, Doranz BJ, Chen RE, Shi PY,
798 Carnahan RH, Thackray LB, Diamond MS, Crowe JE, Jr. 2021. Neutralizing and
799 protective human monoclonal antibodies recognizing the N-terminal domain of the
800 SARS-CoV-2 spike protein. Cell 184:2316-2331 e15.
801 18. Wang N, Sun Y, Feng R, Wang Y, Guo Y, Zhang L, Deng YQ, Wang L, Cui Z, Cao L,
802 Zhang YJ, Li W, Zhu FC, Qin CF, Wang X. 2021. Structure-based development of
803 human antibody cocktails against SARS-CoV-2. Cell Res 31:101-103.
804 19. Shah P, Canziani GA, Carter EP, Chaiken I. 2021. The Case for S2: The Potential
805 Benefits of the S2 Subunit of the SARS-CoV-2 Spike Protein as an Immunogen in
806 Fighting the COVID-19 Pandemic. Front Immunol 12:637651.
807 20. Nguyen-Contant P, Embong AK, Kanagaiah P, Chaves FA, Yang H, Branche AR,
808 Topham DJ, Sangster MY. 2020. S Protein-Reactive IgG and Memory B Cell Production
809 after Human SARS-CoV-2 Infection Includes Broad Reactivity to the S2 Subunit. mBio
810 11.
811 21. Steffen HA, Swartz SR, Jackson JB, Kenne KA, Ten Eyck PP, Merryman AS, Castaneda
812 CN, Marsden K, Maxwell T, Merrill AE, Krasowski MD, Rysavy MB. 2021. SARS-CoV-2
813 Infection during Pregnancy in a Rural Midwest All-delivery Cohort and Associated
814 Maternal and Neonatal Outcomes. Am J Perinatol 38:614-621.
815 22. Salimi H, Johnson J, Flores MG, Zhang MS, O'Malley Y, Houtman JC, Schlievert PM,
816 Haim H. 2020. The lipid membrane of HIV-1 stabilizes the viral envelope glycoproteins
817 and modulates their sensitivity to antibody neutralization. J Biol Chem 295:348-362.

818 23. Johnson J, Flores MG, Rosa J, Han C, Salvi AM, DeMali KA, Jagnow JR, Sparks A,
819 Haim H. 2020. The High Content of Fructose in Human Semen Competitively Inhibits
820 Broad and Potent Antivirals That Target High-Mannose Glycans. J Virol 94.
821 24. Johnson J, Zhai Y, Salimi H, Espy N, Eichelberger N, DeLeon O, O'Malley Y, Courter J,
822 Smith AB, 3rd, Madani N, Sodroski J, Haim H. 2017. Induction of a Tier-1-Like
823 Phenotype in Diverse Tier-2 Isolates by Agents That Guide HIV-1 Env to Perturbation-
824 Sensitive, Nonnative States. J Virol 91.
825 25. Amanat F, Thapa M, Lei T, Ahmed SMS, Adelsberg DC, Carreno JM, Strohmeier S,
826 Schmitz AJ, Zafar S, Zhou JQ, Rijnink W, Alshammary H, Borcherding N, Reiche AG,
827 Srivastava K, Sordillo EM, van Bakel H, Personalized Virology I, Turner JS, Bajic G,
828 Simon V, Ellebedy AH, Krammer F. 2021. The plasmablast response to SARS-CoV-2
829 mRNA vaccination is dominated by non-neutralizing antibodies that target both the NTD
830 and the RBD. medRxiv doi:10.1101/2021.03.07.21253098.
831 26. Liu L, Wang P, Nair MS, Yu J, Rapp M, Wang Q, Luo Y, Chan JF, Sahi V, Figueroa A,
832 Guo XV, Cerutti G, Bimela J, Gorman J, Zhou T, Chen Z, Yuen KY, Kwong PD, Sodroski
833 JG, Yin MT, Sheng Z, Huang Y, Shapiro L, Ho DD. 2020. Potent neutralizing antibodies
834 against multiple epitopes on SARS-CoV-2 spike. Nature 584:450-456.
835 27. Jungbauer C, Weseslindtner L, Weidner L, Gansdorfer S, Farcet MR, Gschaider-
836 Reichhart E, Kreil TR. 2020. Characterization of 100 sequential SARS-CoV-2
837 convalescent plasma donations. Transfusion doi:10.1111/trf.16119.
838 28. Brochot E, Demey B, Touze A, Belouzard S, Dubuisson J, Schmit JL, Duverlie G,
839 Francois C, Castelain S, Helle F. 2020. Anti-spike, Anti-nucleocapsid and Neutralizing
840 Antibodies in SARS-CoV-2 Inpatients and Asymptomatic Individuals. Front Microbiol
841 11:584251.
842 29. Gniadek TJ, Thiede JM, Matchett WE, Gress AR, Pape KA, Fiege JK, Jenkins MK,
843 Menachery VD, Langlois RA, Bold TD. 2020. SARS-CoV-2 neutralization and serology

844 testing of COVID-19 convalescent plasma from donors with nonsevere disease.
845 Transfusion doi:10.1111/trf.16101.
846 30. Case JB, Rothlauf PW, Chen RE, Liu Z, Zhao H, Kim AS, Bloyet LM, Zeng Q, Tahan S,
847 Droit L, Ilagan MXG, Tartell MA, Amarasinghe G, Henderson JP, Miersch S, Ustav M,
848 Sidhu S, Virgin HW, Wang D, Ding S, Corti D, Theel ES, Fremont DH, Diamond MS,
849 Whelan SPJ. 2020. Neutralizing Antibody and Soluble ACE2 Inhibition of a Replication-
850 Competent VSV-SARS-CoV-2 and a Clinical Isolate of SARS-CoV-2. Cell Host Microbe
851 28:475-485 e5.
852 31. Klein SL, Pekosz A, Park HS, Ursin RL, Shapiro JR, Benner SE, Littlefield K, Kumar S,
853 Naik HM, Betenbaugh MJ, Shrestha R, Wu AA, Hughes RM, Burgess I, Caturegli P,
854 Laeyendecker O, Quinn TC, Sullivan D, Shoham S, Redd AD, Bloch EM, Casadevall A,
855 Tobian AA. 2020. Sex, age, and hospitalization drive antibody responses in a COVID-19
856 convalescent plasma donor population. J Clin Invest 130:6141-6150.
857 32. Berger Rentsch M, Zimmer G. 2011. A vesicular stomatitis virus replicon-based bioassay
858 for the rapid and sensitive determination of multi-species type I interferon. PLoS One
859 6:e25858.
860 33. Muecksch F, Wise H, Batchelor B, Squires M, Semple E, Richardson C, McGuire J,
861 Clearly S, Furrie E, Greig N, Hay G, Templeton K, Lorenzi JCC, Hatziioannou T, Jenks
862 S, Bieniasz PD. 2021. Longitudinal Serological Analysis and Neutralizing Antibody
863 Levels in Coronavirus Disease 2019 Convalescent Patients. J Infect Dis 223:389-398.
864 34. Patel EU, Bloch EM, Clarke W, Hsieh YH, Boon D, Eby Y, Fernandez RE, Baker OR,
865 Keruly M, Kirby CS, Klock E, Littlefield K, Miller J, Schmidt HA, Sullivan P, Piwowar-
866 Manning E, Shrestha R, Redd AD, Rothman RE, Sullivan D, Shoham S, Casadevall A,
867 Quinn TC, Pekosz A, Tobian AAR, Laeyendecker O. 2021. Comparative Performance of
868 Five Commercially Available Serologic Assays To Detect Antibodies to SARS-CoV-2
869 and Identify Individuals with High Neutralizing Titers. J Clin Microbiol 59.

870 35. Tang MS, Case JB, Franks CE, Chen RE, Anderson NW, Henderson JP, Diamond MS,
871 Gronowski AM, Farnsworth CW. 2020. Association between SARS-CoV-2 neutralizing
872 antibodies and commercial serological assays. Clin Chem
873 doi:10.1093/clinchem/hvaa211.
874 36. Niu L, Wittrock KN, Clabaugh GC, Srivastava V, Cho MW. 2021. A Structural Landscape
875 of Neutralizing Antibodies Against SARS-CoV-2 Receptor Binding Domain. Front
876 Immunol 12:647934.
877 37. Seydoux E, Homad LJ, MacCamy AJ, Parks KR, Hurlburt NK, Jennewein MF, Akins NR,
878 Stuart AB, Wan YH, Feng J, Whaley RE, Singh S, Boeckh M, Cohen KW, McElrath MJ,
879 Englund JA, Chu HY, Pancera M, McGuire AT, Stamatatos L. 2020. Analysis of a SARS-
880 CoV-2-Infected Individual Reveals Development of Potent Neutralizing Antibodies with
881 Limited Somatic Mutation. Immunity 53:98-105 e5.
882 38. Amanat F, Thapa M, Lei T, Ahmed SMS, Adelsberg DC, Carreno JM, Strohmeier S,
883 Schmitz AJ, Zafar S, Zhou JQ, Rijnink W, Alshammary H, Borcherding N, Reiche AG,
884 Srivastava K, Sordillo EM, van Bakel H, Personalized Virology I, Turner JS, Bajic G,
885 Simon V, Ellebedy AH, Krammer F. 2021. SARS-CoV-2 mRNA vaccination induces
886 functionally diverse antibodies to NTD, RBD, and S2. Cell
887 doi:10.1016/j.cell.2021.06.005.
888 39. Collier DA, De Marco A, Ferreira I, Meng B, Datir RP, Walls AC, Kemp SA, Bassi J,
889 Pinto D, Silacci-Fregni C, Bianchi S, Tortorici MA, Bowen J, Culap K, Jaconi S,
890 Cameroni E, Snell G, Pizzuto MS, Pellanda AF, Garzoni C, Riva A, Collaboration C-
891 NBC-, Elmer A, Kingston N, Graves B, McCoy LE, Smith KGC, Bradley JR, Temperton
892 N, Ceron-Gutierrez L, Barcenas-Morales G, Consortium C-GU, Harvey W, Virgin HW,
893 Lanzavecchia A, Piccoli L, Doffinger R, Wills M, Veesler D, Corti D, Gupta RK. 2021.
894 Sensitivity of SARS-CoV-2 B.1.1.7 to mRNA vaccine-elicited antibodies. Nature
895 593:136-141.

40. Voss WN, Hou YJ, Johnson NV, Delidakis G, Kim JE, Javanmardi K, Horton AP, Bartzoka F, Paresi CJ, Tanno Y, Chou CW, Abbasi SA, Pickens W, George K, Boutz DR, Towers DM, McDaniel JR, Billick D, Goike J, Rowe L, Batra D, Pohl J, Lee J, Gangappa S, Sambhara S, Gadush M, Wang N, Person MD, Iverson BL, Gollihar JD, Dye JM, Herbert AS, Finkelstein IJ, Baric RS, McLellan JS, Georgiou G, Lavinder JJ, Ippolito GC. 2021. Prevalent, protective, and convergent IgG recognition of SARS-CoV-2 non-RBD spike epitopes. Science 372:1108-1112.

41. Jaaskelainen AJ, Kuivanen S, Kekalainen E, Ahava MJ, Loginov R, Kallio-Kokko H, Vapalahti O, Jarva H, Kurkela S, Lappalainen M. 2020. Performance of six SARS-CoV-2 immunoassays in comparison with microneutralisation. J Clin Virol 129:104512.

42. Luchsinger LL, Ransegnola B, Jin D, Muecksch F, Weisblum Y, Bao W, George PJ, Rodriguez M, Tricoche N, Schmidt F, Gao C, Jawahar S, Pal M, Schnall E, Zhang H, Strauss D, Yazdanbakhsh K, Hillyer CD, Bieniasz PD, Hatziioannou T. 2020. Serological Assays Estimate Highly Variable SARS-CoV-2 Neutralizing Antibody Activity in Recovered COVID19 Patients. J Clin Microbiol doi:10.1128/JCM.02005-20.

43. Grenache DG, Ye C, Bradfute SB. 2020. Correlation of SARS-CoV-2 neutralizing antibodies to an automated chemiluminescent serological immunoassay. J Appl Lab Med doi:10.1093/jalm/jfaa195.

44. Rychert J, Couturier MR, Elgort M, Lozier BK, La'ulu S, Genzen JR, Straseski JA, Delgado JC, Slev PR. 2020. Evaluation of Three SARS CoV-2 IgG Antibody Assays and Correlation with Neutralizing Antibodies. J Appl Lab Med doi:10.1093/jalm/jfaa188.

45. Haim H, Salas I, Sodroski J. 2013. Proteolytic processing of the human immunodeficiency virus envelope glycoprotein precursor decreases conformational flexibility. J Virol 87:1884-9.

920 46. Cervera L, Gonzalez-Dominguez I, Segura MM, Godia F. 2017. Intracellular
921 characterization of Gag VLP production by transient transfection of HEK 293 cells.
922 Biotechnol Bioeng 114:2507-2517.

923

Figure 1

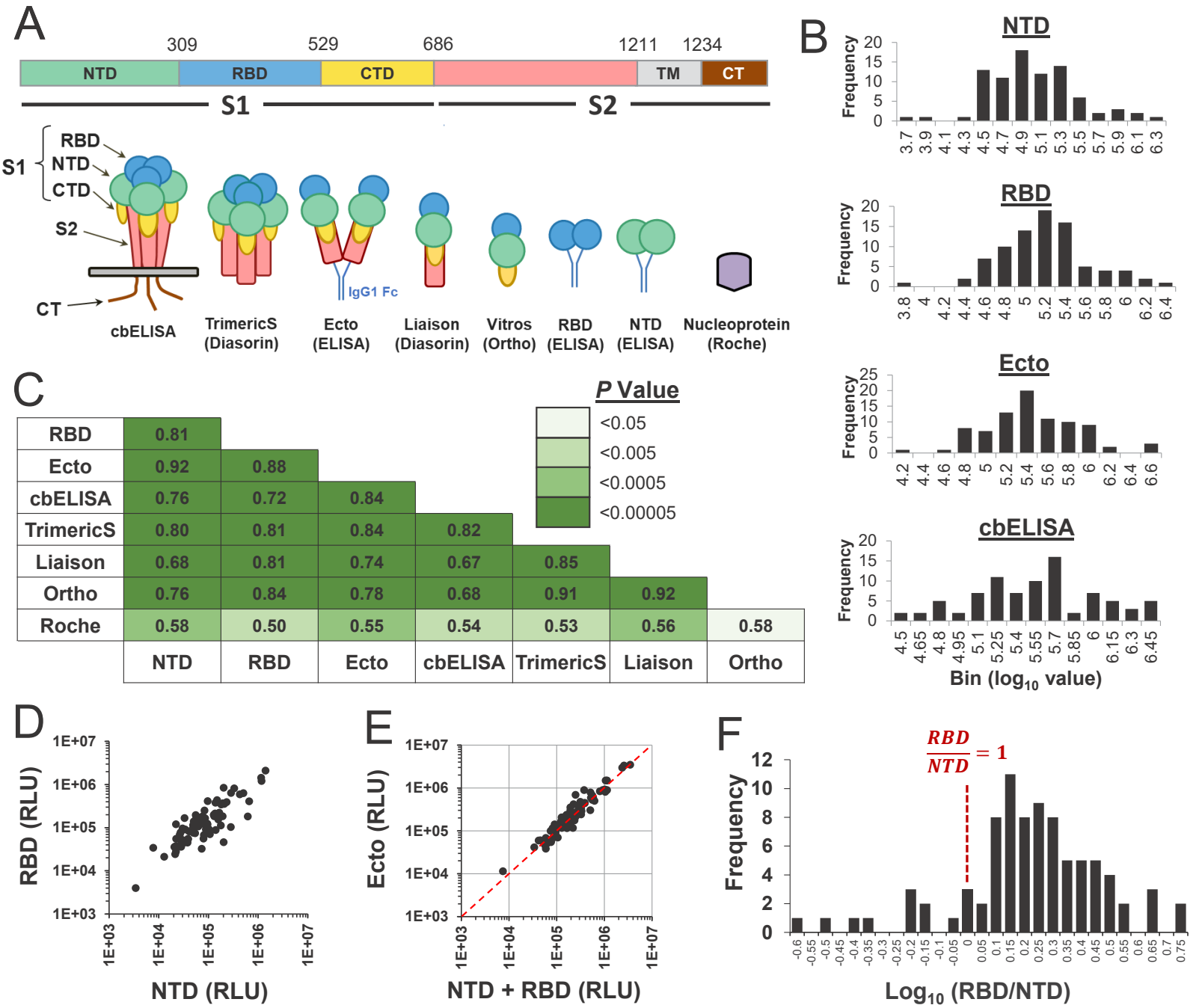

Figure 2

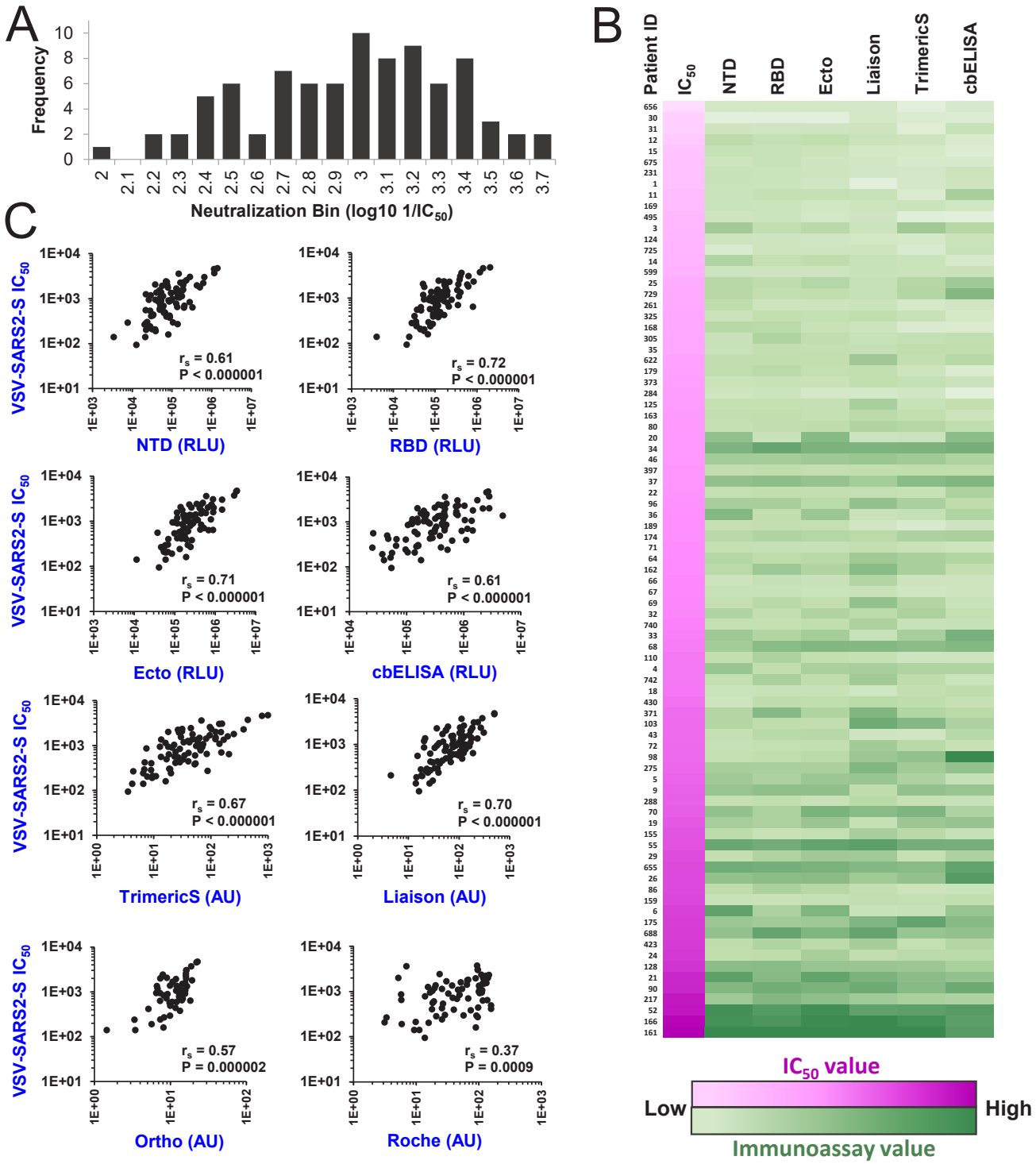

Figure 3

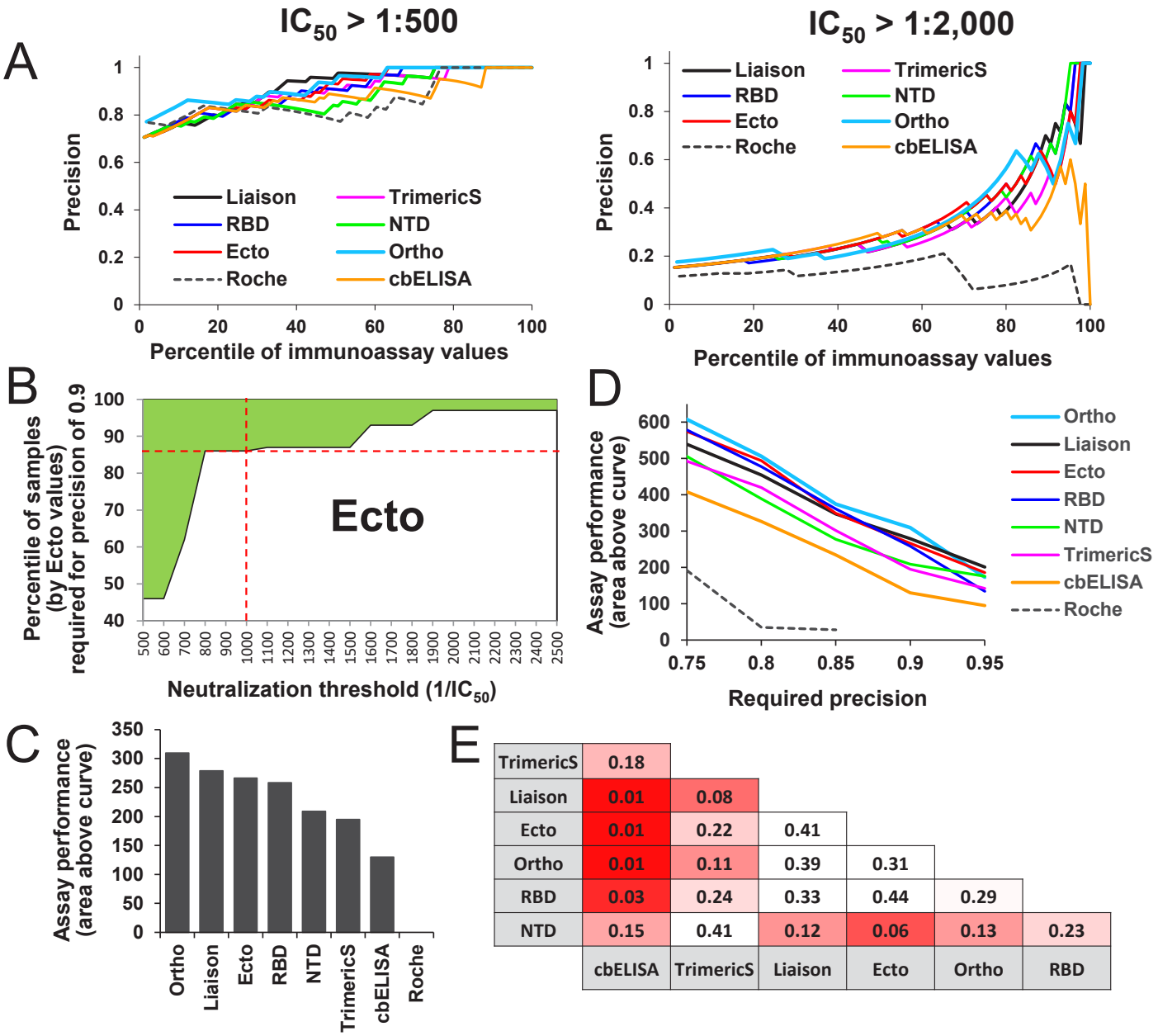

Figure 4

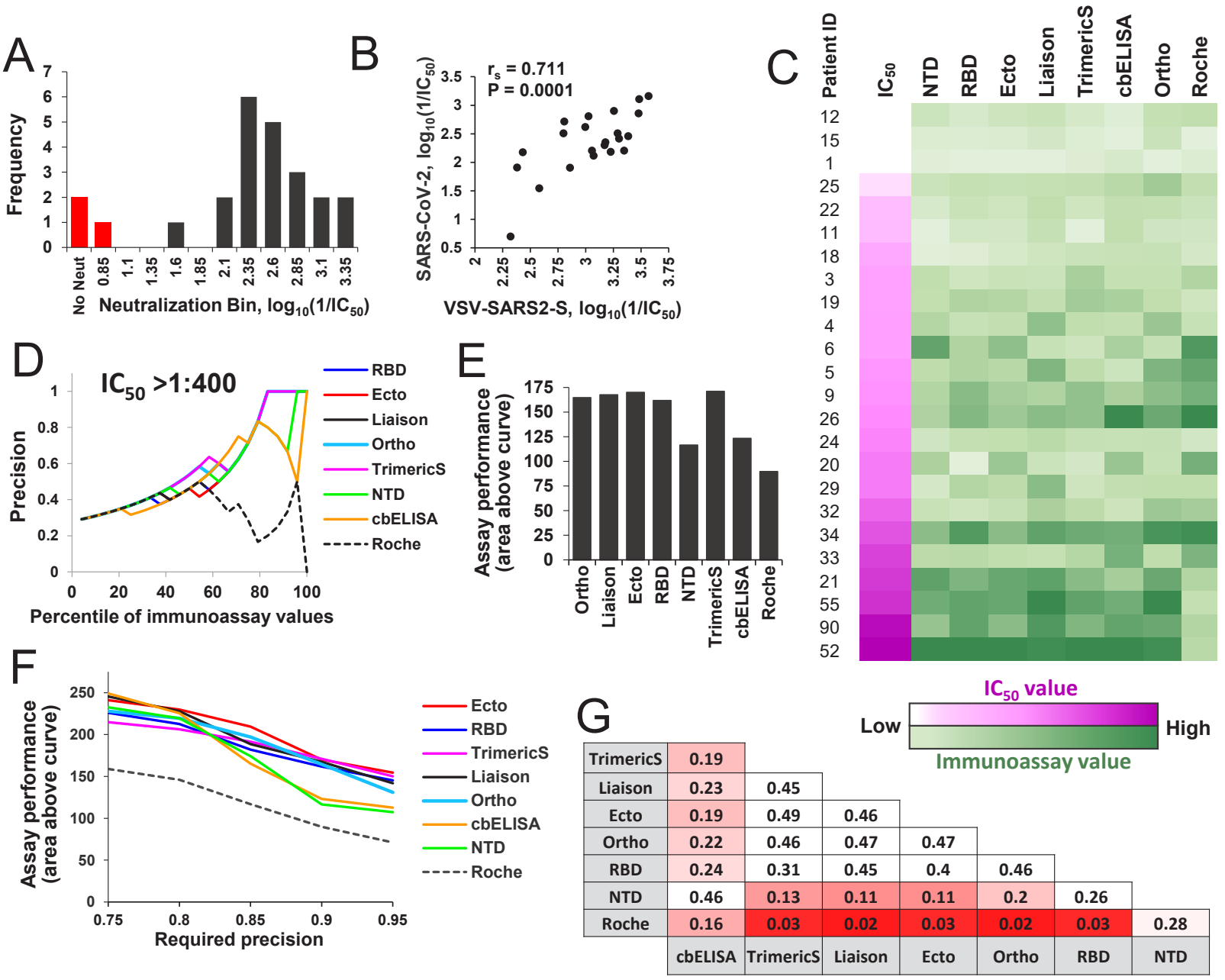

TrimericS	0.19						
Liaison	0.23	0.45					
Ecto	0.19	0.49	0.46				
Ortho	0.22	0.46	0.47	0.47			
RBD	0.24	0.31	0.45	0.4	0.46		
NTD	0.46	0.13	0.11	0.11	0.2	0.26	
Roche	0.16	0.03	0.02	0.03	0.02	0.03	0.28
	cbELISA	TrimericS	Liaison	Ecto	Ortho	RBD	NTD

Figure 5

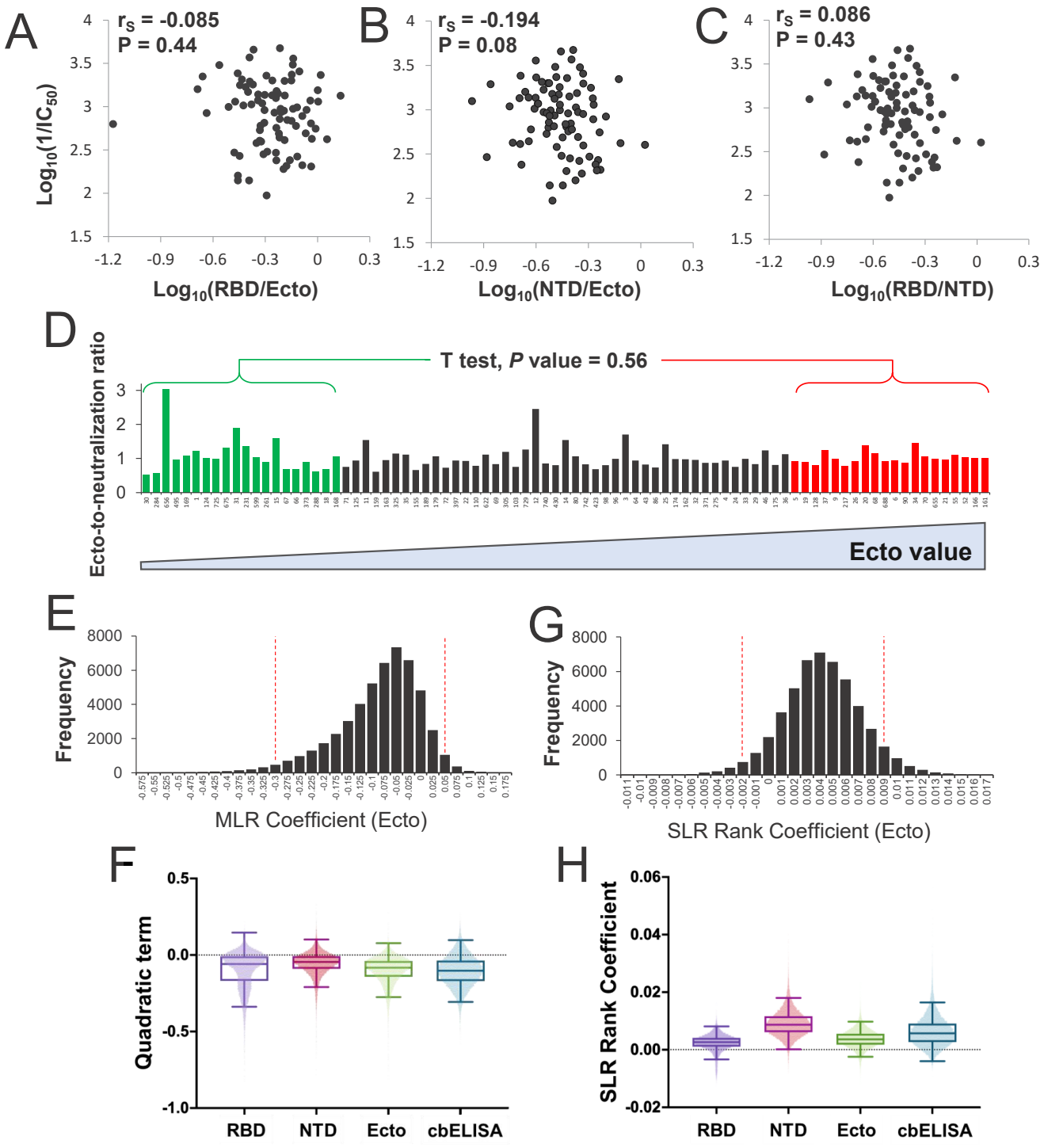

Figure 6

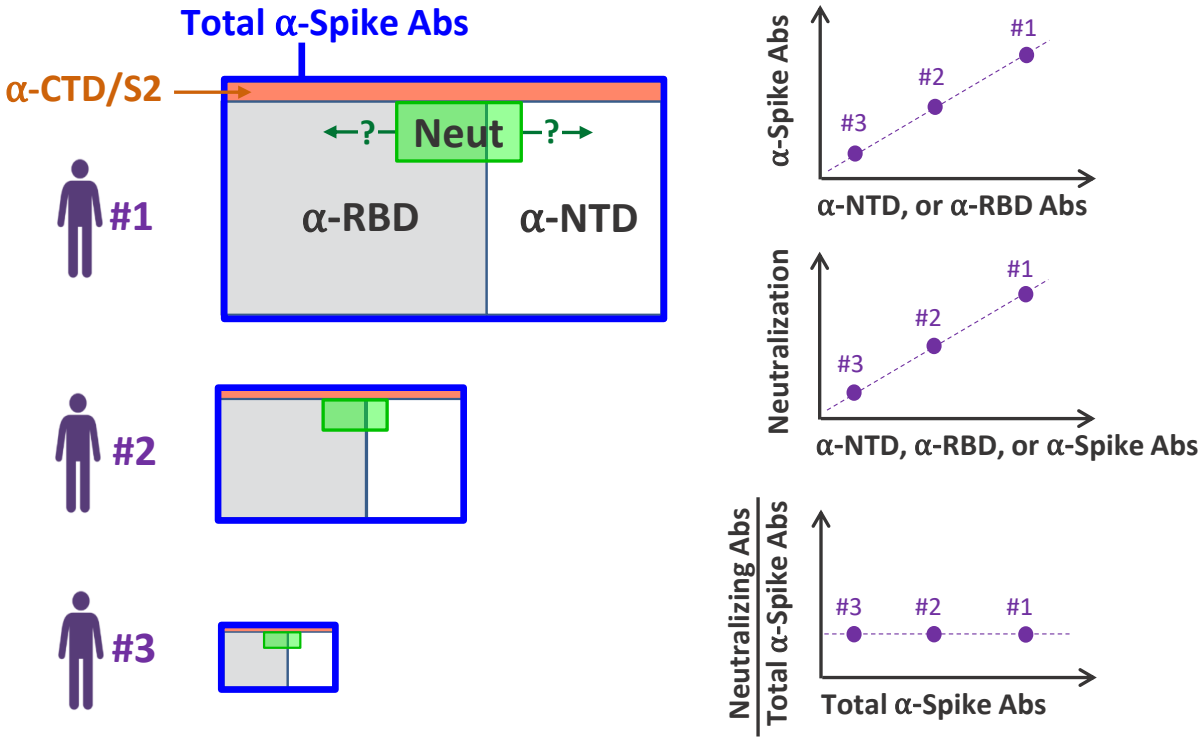

Supplemental Figure S1

A

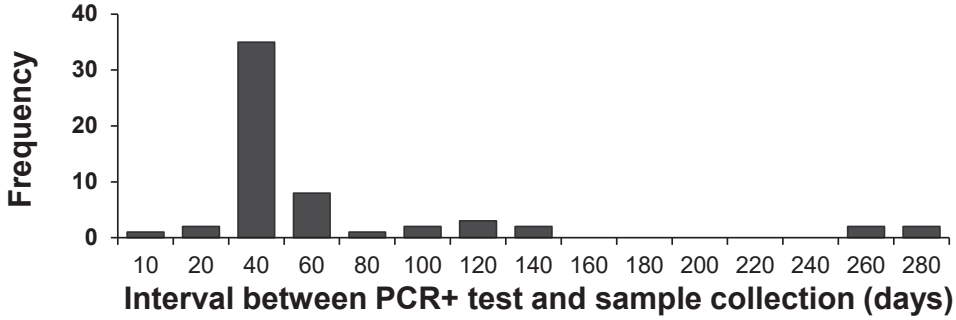

B

	P value	*P* value for log_{10}-transformed data
NTD	<0.0001	0.11
RBD	<0.0001	0.08
Ecto	<0.0001	0.29
Liaison	<0.0001	0.56
Ortho	0.82	<0.0001
TrimericS	<0.0001	0.67
Roche	<0.0001	<0.0001
cbELISA	<0.0001	0.76

C

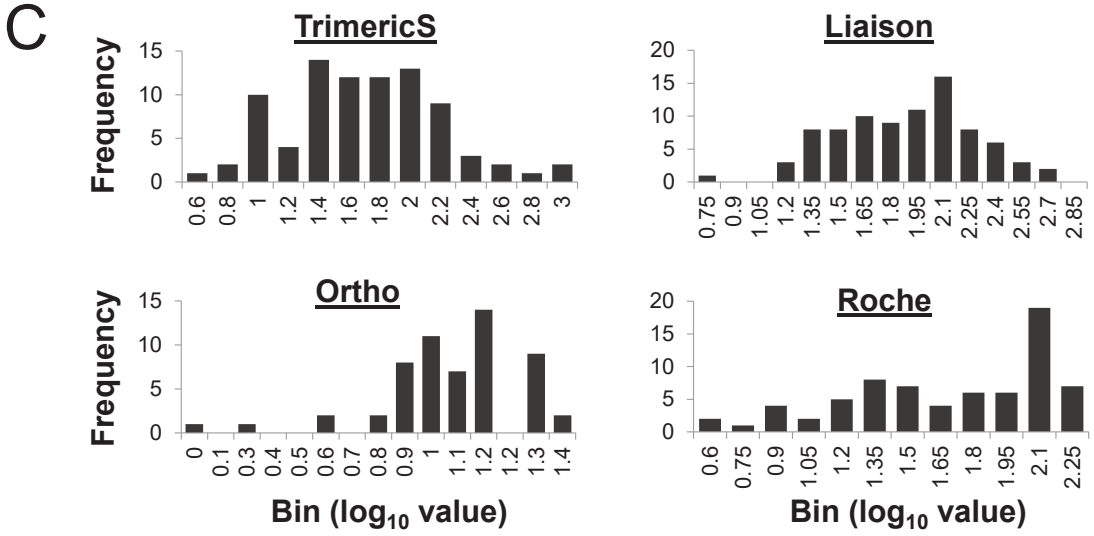

Supplemental Figure S2

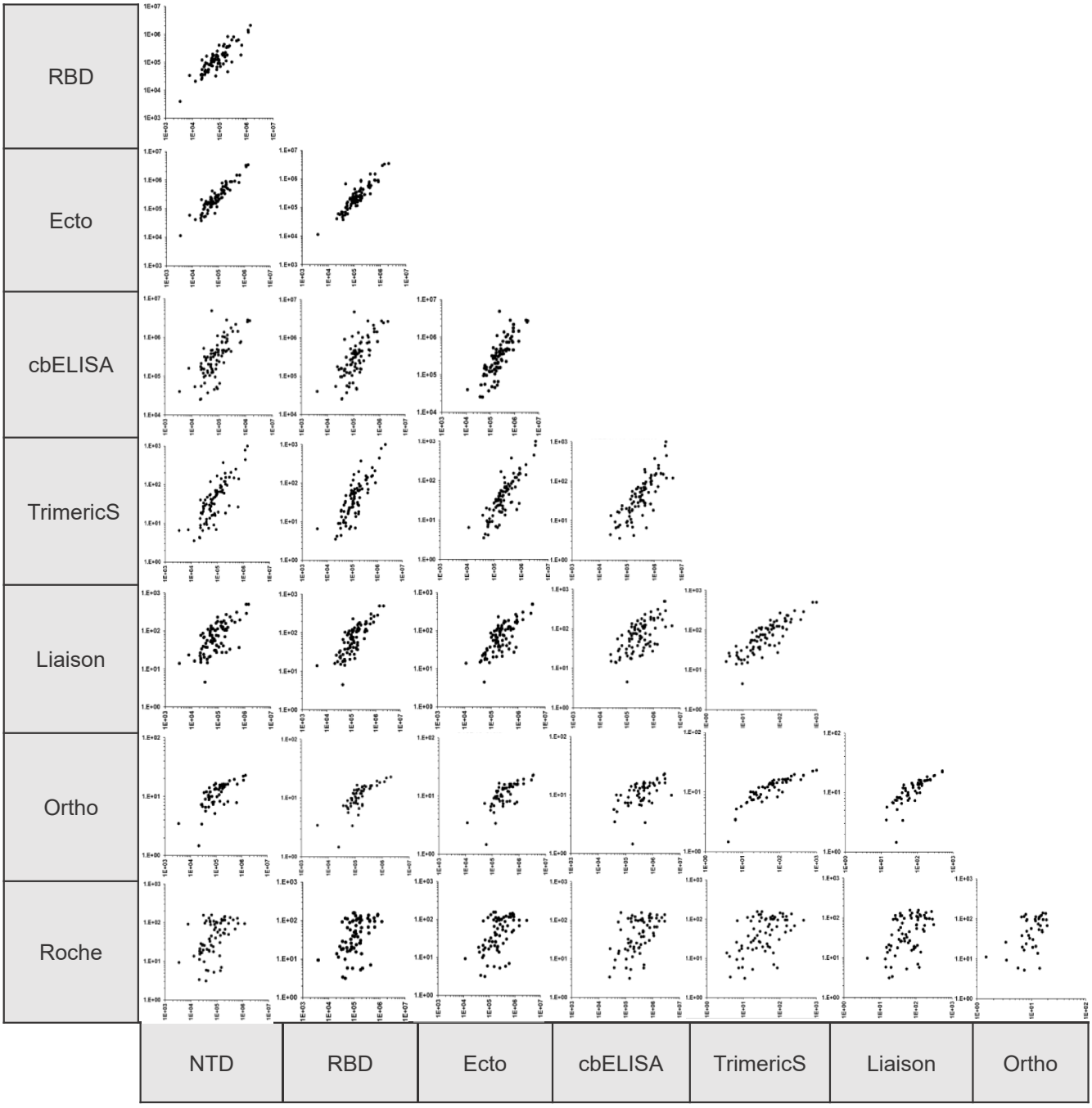

Supplemental Figure S3

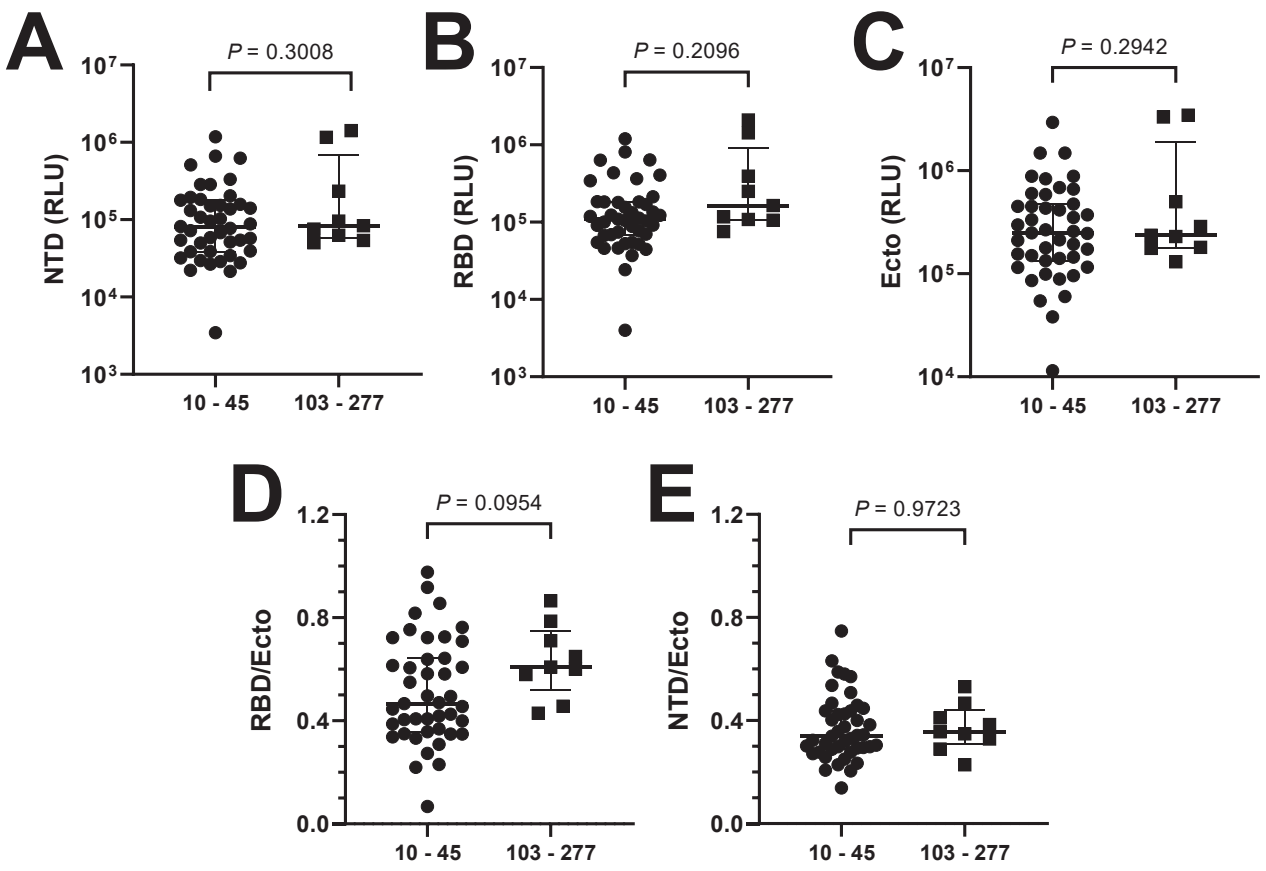

Supplemental Figure S4

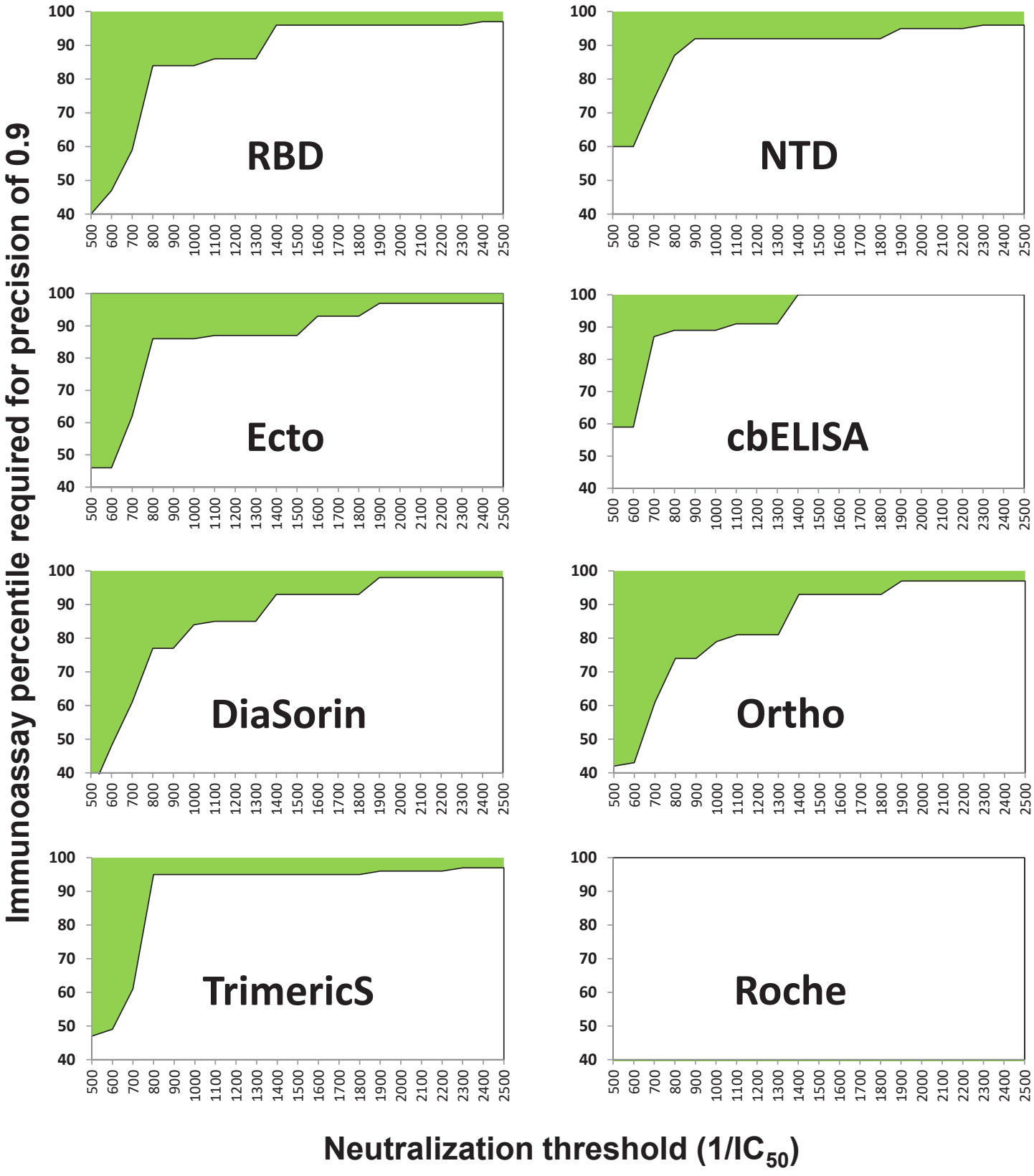

Supplemental Figure S5

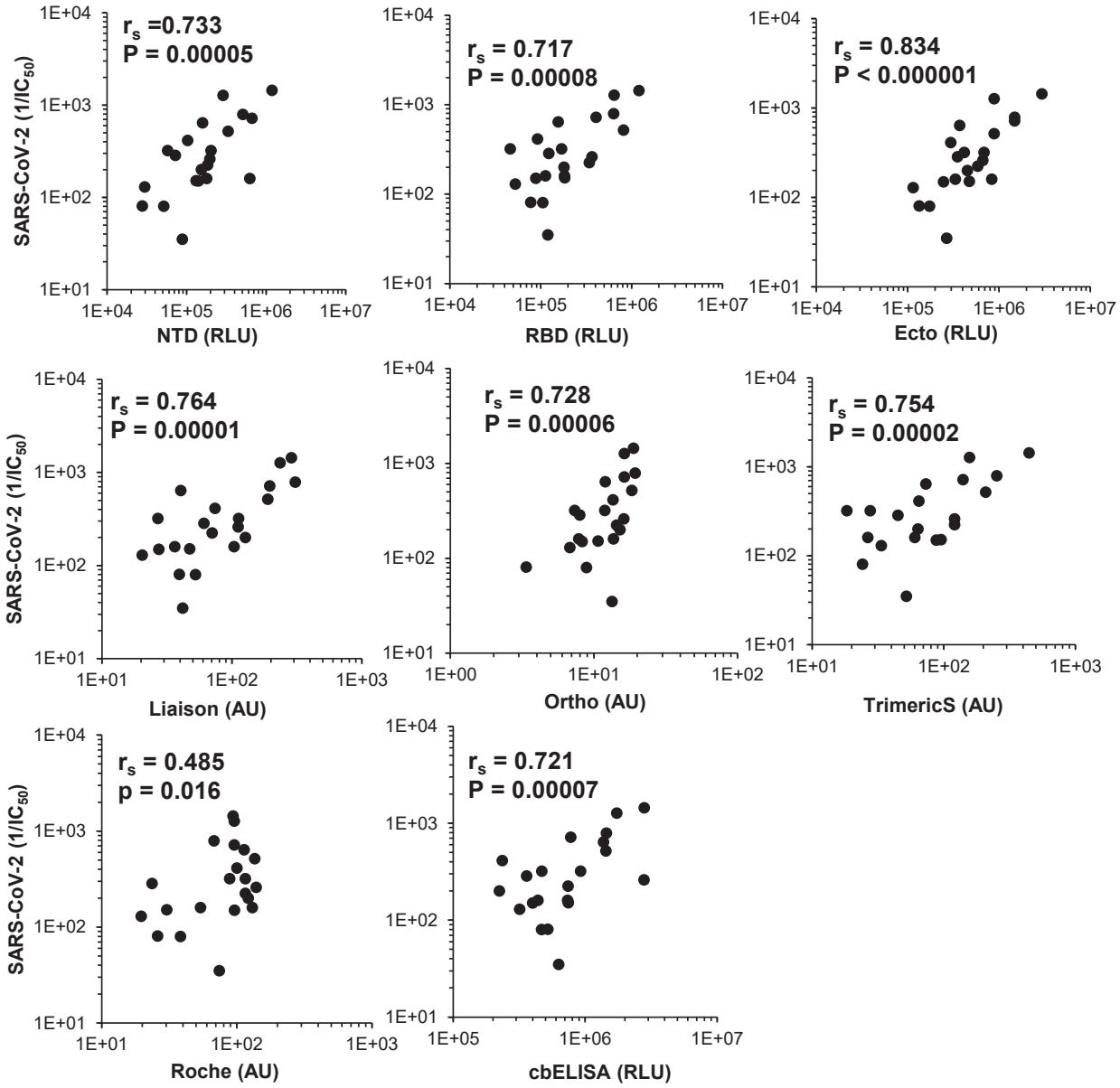

Supplemental Figure S6